Article:

1   **PBP1 of *Staphylococcus aureus* has multiple essential functions in cell**

2   **division**

3

4   Katarzyna Wacnik[1,2], Vincenzo A Rao[3], Xinyue Chen[2,4], Lucia Lafage[1,2], Manuel Pazos[5],

5   Simon Booth[3], Waldemar Vollmer[5], Jamie K Hobbs[2,4], Richard J Lewis[3‡] and Simon J

6   Foster[1,2*]

7

8   [1] School of Biosciences, University of Sheffield, Sheffield, UK

9   [2] The Florey Institute for Host-Pathogen Interactions, University of Sheffield, Sheffield, UK

10   [3] Biosciences Institute, Newcastle University, Newcastle upon Tyne, UK.

11   [4] Department of Physics and Astronomy, University of Sheffield, Sheffield, UK

12   [5] Centre for Bacterial Cell Biology, Bioscience Institute, Newcastle University, Newcastle

13   upon Tyne, UK.

14

15   [‡] Current address: The Royal Society for the Protection of Birds, The Lodge, Sandy,

16   Bedfordshire SG19 2DL

17   * To whom correspondence should be sent. E-mail: s.foster@sheffield.ac.uk.

Abstract

Bacterial cell division is a complex process requiring the coordination of multiple components, to allow the appropriate spatial and temporal control of septum formation and cell scission. Peptidoglycan (PG) is the major structural component of the septum, and our recent studies in the human pathogen *Staphylococcus aureus* have revealed a complex, multi-stage PG architecture that develops during septation. Penicillin binding proteins (PBPs) are essential for the final steps of PG biosynthesis – their transpeptidase activity links together the peptide sidechain of nascent glycan strands together. PBP1 is required for cell division in *S. aureus* and here we demonstrate that it has multiple essential functions associated with its enzymatic activity and as a regulator of division. Loss of PBP1, or just its C-terminal PASTA domains, results in cessation of division at the point of septal plate formation. The PASTA domains can bind PG and thus coordinate the cell division process. The transpeptidase activity of PBP1 is also essential but its loss leads to a strikingly different phenotype of thickened and aberrant septa, which is phenocopied by the morphological effects of adding the PBP1-specific β-lactam, meropenem. Together these results lead to a model for septal PG synthesis where PBP1 enzyme activity is responsible for the characteristic architecture of the septum and PBP1 protein molecules coordinate cell division allowing septal plate formation.

Introduction

Peptidoglycan (PG) is the major structural component of the bacterial cell wall and is essential for maintaining cell shape, integrity and survival (Silhavy et al., 2010; Turner et al., 2014; Vollmer et al., 2008). The final assembly stages of assembly of this large polymeric molecule are mediated by penicillin-binding proteins (PBPs), key PG synthases that, through their transglycosylase (TG) and transpeptidase (TP) activities, polymerise glycan chains and cross-link them into a mesh-like hydrogel (Pasquina-Lemonche et al., 2020; Typas et al.,

2

43   2011). Since the cell wall is essential for maintaining bacterial life, PBPs and PG synthesis

44   are a target of some of the most important antibiotics, β-lactams (penicillins) and

45   glycopeptides (vancomycin) (Schneider & Sahl, 2010; Zapun et al., 2008). The major human

46   pathogen *Staphylococcus aureus* has a minimalist PBP system as it encodes only four PBPs,

47   PBP1 to PBP4 (Pinho et al., 2013). Only PBP1 (class B PBP with only TP activity, bPBP)

48   and PBP2 (class A bifunctional PBP with both TG and TP activities, aPBP) are essential and

49   sufficient for septal and peripheral PG synthesis in *S. aureus* (Lund et al., 2018; Pinho et al.,

50   2013). PBP2 is the major PG synthase of *S. aureus*, and the septal formation activity of PBP2

51   is mediated by its substrate, Lipid II (Pinho & Errington, 2005). Although PBP2 is essential,

52   loss of its TP activity can be compensated for by a horizontally acquired class B PBP2A in

53   methicillin-resistant *S. aureus* (MRSA) (Pinho, Filipe, et al., 2001). PBP2A, however, cannot

54   replace PBP1, whose loss is detrimental to the viability of *S. aureus* (Pereira et al., 2007).

55   PBP1 and PBP3 form cognate pairs with the monofunctional TGs, FtsW and RodA,

56   belonging to the SEDS (shape, elongation, division and sporulation) family (Meeske et al.,

57   2016) to facilitate septum formation (PBP1-FtsW) and to maintain the prolate cell shape

58   (PBP3-RodA) of *S. aureus*, respectively (Reichmann et al., 2019). PBP4 is a class C PBP

59   with D,D-carboxypeptidase activity (cPBP) and has a TP activity that contributes to the high-

60   level cross-linking of PG and MRSA resistance to β-lactams (Loskill et al., 2014; Srisuknimit

61   et al., 2017).

62

63   Although *S. aureus* PBPs have been studied over many years, the specific roles of PBP1 in

64   cell division, PG synthesis and architecture have remained elusive. Previous studies have

65   shown that whilst PBP1 is essential, its TP activity is not, implying another role (Pereira et

66   al., 2007; Reichmann et al., 2019). However, this work was performed in an MRSA

67   background that contains PBP2A, encoded by *mecA*, which is non-native to *S. aureus* (Pinho,

68   de Lencastre, et al., 2001). Whilst PBP2A cannot replace PBP1, how these proteins interact is

69   unknown. We have recently shown that the presence of *mecA* has a profound effect on

70   cellular physiology (Panchal et al., 2020). Thus it is important to understand individual and

71   combined roles of *S. aureus* PBPs both in the presence and absence of the exogenous PBP2A,

72   as the vast majority of *S. aureus* infections are caused by methicillin sensitive strains.

73

74   **Results**

75   ***S. aureus* PBP1 PASTA domains are essential for growth and PBP1 functionality**

76   PBP1 has a cytoplasmic N-terminal region, a membrane spanning sequence, an

77   exocytoplasmic dimerization domain and a C-terminal region consisting of the TP domain

78   and two PASTA domains (for penicillin-binding protein and serine/threonine kinase

79   associated domain) (Yeats et al., 2002). We created a set of conditional mutants of *pbp1* to

80   investigate the role of PBP1 in cell division and PG synthesis. An ectopic copy of *pbp1* under

81   the control of the P*spac* promoter (P$_{spac}$-*pbp1*) was placed at the lipase locus (*geh*::P$_{spac}$-*pbp1*)

82   of *S. aureus* SH1000, and a series of changes were made in this genetic background at the

83   native *pbp1* locus: (i) an in-frame deletion of *pbp1* (Δ*pbp1)*, (ii) a deletion of the region

84   encoding the two PASTA domains (*pbp1*Δ$_{PASTA}$)*, and (iii) the substitution of the catalytic

85   Ser314 to Ala in the TP domain (*pbp1**) (Fig. 1a, b). We examined the essentiality of PBP1,

86   the PASTA domains and the active TP domain with these mutants. Depletion of PBP1 via

87   IPTG removal (Fig. 1c and Fig. 1 – figure supplement 1a, b) resulted in cell death,

88   confirming the essentiality of PBP1 (Fig. 1c, d and Fig. 1 – figure supplement 1c, d,).

89   Deletion of the PASTA domains also led to growth inhibition and more than 99% cell death

90   within 4 h (Fig. 1d and Fig. 1 – figure supplement 1c, d). Importantly, this phenotype was not

91   associated with PBP1$_{ΔPASTA}$ instability (Fig. 1c and Fig. 1 – figure supplement 1a) or loss of

92   its ability to bind its substrate analogue BocillinFL (Fig. 1 – figure supplement 1b). By

4

93   contrast, deletion of the PASTA domains of *Streptococcus pneumoniae* PBP2x, a PBP1

94   orthologue, resulted in a complete loss of BocillinFL binding (Maurer et al., 2012). These

95   results indicate the PASTA domains are essential for *S. aureus* growth and PBP1

96   functionality but not its enzymatic activity.

97   During construction of the *pbp1** mutant we obtained, by serendipity, a *pbp1*$_{STOP}$ mutant in

98   which a SNP in the codon for Glu292 resulted in its replacement with a premature stop codon

99   and the truncation of the entire TP and PASTAs region of PBP1 (Fig. 1 – figure supplement

100   1e, f). However, immunoblot analysis using anti-PBP1 sera could not confirm the presence of

101   the PBP1$_{STOP}$ protein in the *pbp1*$_{STOP}$ mutant (Fig. 1 – figure supplement 1g), suggesting that

102   stability of the N-terminal domain of PBP1 is dependent on its C-terminus.

103   Although inactivation of PBP1 TP activity (PBP1*) did not affect protein stability (Fig. 1c),

104   it did remove the ability of PBP1 to bind BocillinFL (Fig. 1 – figure supplement 1b). The loss

105   of PBP1 TP activity resulted in severely compromised growth on solid media (Fig. 1d and

106   Fig. 1 – figure supplement 1c) and reduced cellular viability in liquid culture (Fig. 1e and Fig.

107   1 – figure supplement 1d). Thus, the TP activity of PBP1 is required for growth in the

108   SH1000 background. Inactivation of the PBP1 TP activity was reported previously not to

109   affect growth in the COL strain background (Reichmann et al., 2019). The differences in the

110   necessity for the PBP1 TP activity could result from COL being MRSA whereas SH1000 is a

111   methicillin sensitive *S. aureus* (MSSA).

112

113   **PBP1 TP activity is crucial in MSSA but not in MRSA**

114   We have recently developed a set of defined strains where high-level β-lactam resistance of

115   MRSA is mediated by *mecA* encoding PBP2A and a mutation in either *rpoB* or *rpoC*

116   (Panchal et al., 2020). This combination of genetic alterations (*mecA*$^+$ *rpoB*) are present in

117   COL (Panchal et al., 2020). To test if the apparent disparity in PBP1 role is associated with

118 MRSA, we developed a high-level resistant mutant of *pbp1** in the well-characterised *S.*

119 *aureus* SH1000 by adding the *mecA rpoB*^{H929Q} to the MSSA *pbp1** mutant, resulting in

120 SH1000$_{MRSA}$ *pbp1** (Fig. 1 – figure supplement 2a). Inactivating PBP1 TP did not affect the

121 ability of SH1000$_{MRSA}$ *pbp1** to grow in the absence of IPTG, whereas *pbp1* depletion led to

122 growth inhibition in the isogenic Δ*pbp1* MSSA and MRSA strains (Fig. 1d, e and Fig. 1 –

123 figure supplement 2b-d). Thus, the fundamental role of PBP1 in growth and division can only

124 be studied in an MSSA background as otherwise the role of PBP1 can be confounded by the

125 presence of the MRSA resistance apparatus.

126

127 **PBP1 PASTA domains are required for septum progression**

128 PG synthesis still occurred in Δ*pbp1*, *pbp1*$_{ΔPASTA}$ and *pbp1** in the absence of IPTG, despite

129 cell growth inhibition, as measured by the incorporation of the fluorescent D-amino acid

130 derivative HADA (Fig. 2a). This was not a consequence of the non-synthesis, exchange

131 reaction carried out by PBP4 as it occurred in *pbp4* as well as with the dipeptide ADA-DA

132 (Kuru et al., 2019; Lund et al., 2018) (Fig. 2 – figure supplement 1). All variants increased in

133 cell volume upon depletion of *pbp1*, whereas *pbp1*$_{ΔPASTA}$ was enlarged by almost twice as

134 much as Δ*pbp1* and *pbp1** (Fig. 2a, b and Fig. 2 – figure supplement 2a). Despite differences

135 in cell size, both Δ*pbp1* and *pbp1*$_{ΔPASTA}$ decreased the number of cells with complete septa

136 (Fig. 2a, c). Transmission electron microscopy (TEM) showed that more than 80% of the

137 population had growth defects including cell wall thickening, PG blebs, mis-shapen and/or

138 multiple, incomplete septa. (Fig 2d, e and Fig. 2 – figure supplement 2b, c). Such septa had

139 abnormally thick bases and sharply pointed leading edges, suggesting that cell growth arrest

140 was not due to a lack of septal initiation but instead arrest of inward septum progression.

141 Atomic force microscopy (AFM) has revealed previously that the first step in cell division is

142 the formation of a PG feature called the "piecrust", prior to the septal plate(Turner et al.,

6

143   2010). The *S. aureus* septal plate has two PG architectures: disordered mesh facing the cell

144   membrane and concentric rings in the septum core (Pasquina-Lemonche et al., 2020). Here

145   lack of PBP1 or the PBP1 PASTA domains led to formation of more than one, and often

146   misplaced, piecrust. These mutations also caused an increase in unfinished septal annuli and

147   alterations in the ring surface architecture (Fig 2f and Fig. 2 – figure supplement 3a, c –

148   arrowheads), a characteristic feature of the division plane, freshly revealed immediately after

149   cell scission (Pasquina-Lemonche et al., 2020). Thus, depletion of PBP1 did not stop septum

150   initiation but the loss of the PASTA domains was enough to cause formation of irregular

151   piecrusts, arrest septal plate formation and lead to an altered septal PG architecture.

152

153   **PBP1 TP activity regulates septal PG architecture**

154   The *pbp1** mutant gave a novel phenotype quite distinct from loss of entire PBP1 or the

155   PASTA domains. Inactivation of PBP1 TP activity did not prevent initiation and closing of

156   the septa, but instead resulted in accumulation of cells with aberrant septa and separation

157   defects in about 80% of the population (Fig. 2a, c, e). The septa in such cells had a rounded

158   leading edge, were curved, abnormally thick (Fig. 2d, e and Fig. 2 – figure supplement 2b, c),

159   had agglomerations of mesh-like material close to the septal centre in addition to irregular

160   piecrusts as observed by AFM (Fig. 2f and Fig. 2 – figure supplement 3a, b). The

161   intracellular agglomerations are PG as they stain heavily with HADA and ADA-DA (Fig. 2a

162   and Fig. 2 – figure supplement 1c, f) and could be observed in purified sacculi (Fig. 2f and

163   Fig. 2 – figure supplement 3b). No ring architecture, only mesh structured PG could be

164   observed on the surface of the *pbp1** mutant. Importantly, using fluorescence microscopy the

165   *pbp1* pbp3 pbp4* mutant, in which PBP2 is the only active TP, presented a similar phenotype

166   upon IPTG removal as *pbp1**, exemplified by misshapen septa and agglomerations of PG

167   material marked by HADA (Fig. 2 – figure supplement 2d). Therefore, septal synthesis and

168   progression still occurred in the *pbp1** mutant, however, they resulted from PBP2

169   transpeptidase activity and potentially the transglycosylase activity of FtsW.

170

171   The *pbp1** phenotype occurred specifically because of the loss of the TP activity of this

172   essential enzyme. This phenotype is mirrored by the mode of action of β-lactam antibiotics,

173   which bind to and inhibit the TP activity of PBPs (Schneider & Sahl, 2010). Our results

174   suggest that PBP1 TP activity has a specific role in septal plate formation and without this the

175   septum is mis-shapen. The conditional lethal strains made here allow for functional analysis

176   of the genes concerned. However, phenotypes tend to accumulate on depletion of the wild-

177   type protein over time confusing the precise roles for individual components. To

178   independently corroborate the role of the TP activity of PBP1 we utilized an approach to

179   directly, and selectively, inhibit its activity. Meropenem (MEM) has a higher affinity for

180   PBP1 than PBP2 (Berti et al., 2013; Yang et al., 1995) and, therefore, we hypothesised that

181   its effect on *S. aureus* would match *pbp1**. In a MEM-titration, treatment with 1x MIC MEM

182   was sufficient to lead to cell death and a significant increase in SH1000 WT cell volume after

183   1 h (Fig. 3a, b and Fig. 3 – figure supplement 1a). More than 70% of MEM treated cells had

184   growth defects that manifested as aberrantly shaped septa and accumulation of PG as shown

185   by HADA labelling (Fig. 3a, c, d Fig. 3 – figure supplement 1c, e), similar to observations

186   made with the *pbp1** mutants (Fig. 2a, c-e, Fig. 2 – figure supplement 1c, f). The MEM

187   phenotype of malformed septa was not linked to PBP3 or PBP4 as it was also observed in the

188   corresponding double mutant (Fig. 3c, d and Fig. 3 – figure supplement 1b, d, f), which

189   corroborated the role of PBP2 in misshapen septal genesis.

190

191   **PASTA domains mediate PBP1 interaction with division components**

192   The morphologies of the Δ*pbp1* and *pbp1*_ΔPASTA_ mutants resemble *S. aureus* depleted of

193   DivIB in which EzrA and FtsZ form multiple rings and the synthesis of the cross wall is

194   blocked, despite the normal recruitment of early cell division proteins and piecrust formation

195   (Bottomley et al., 2014). In the Δ*pbp1 ezrA-gfp* mutant, EzrA, which here acts as an early cell

196   division marker, was localised at midcell in the majority of cells and formed additional arcs

197   or rings in 33.5% of the population (Fig. 4a, d). Multiple EzrA rings were observed in 42.7%

198   of the *pbp1*_ΔPASTA_ *ezrA-gfp* mutant cells (Fig. 4b, d), supporting the requirement for PBP1

199   PASTA domains for correct selection of the division site. Alternatively, the multiple division

200   rings could result from a lack of the septal progression whereby the unproductive division

201   machinery results in futile additional alternative initiation attempts, suggesting that PASTA

202   domains are involved in the progression from piecrust to septal plate formation. While the

203   number of cells with complete septa (EzrA-GFP visible as a line or focus) reduced by at least

204   6-fold in Δ*pbp1 ezrA-gfp* and *pbp1*_ΔPASTA_ *ezrA-gfp*, it only halved in *pbp1* ezrA-gfp* (12.5%

205   to 6.3% of *pbp1* ezrA-gfp* in +/-IPTG, respectively; Fig. 4c, d), confirming that septum

206   progression, although reduced, still occurred when PBP1 TP was inactive implying that TP

207   activity is necessary for correct septal architecture during cell division.

208

209   The cell wall of Gram-positive bacteria is decorated with wall teichoic acid (WTA)

210   glycopolymers (Neuhaus & Baddiley, 2003). WTA regulates cell shape, ion homeostasis,

211   autolytic enzymes, growth and division (Swoboda et al., 2010). In *S. aureus*, WTA plays a

212   crucial role in virulence, MRSA resistance to β-lactam antibiotics, PBP4 localisation at the

213   septum and PG cross-linking (Atilano et al., 2010; Campbell et al., 2011; Farha et al., 2013;

214   Weidenmaier et al., 2005). Loss of WTA also results in a proportion of cells with aberrant

215   septa (Campbell et al., 2011) suggesting a link with PBP1 function. Loss of *tarO* (leading to a

216   lack of WTA) caused minor cell division defects in SH1000 (Fig. 4 – figure supplement 1a, e,

217   f). Combining *tarO* with the mutations in *pbp1* exacerbated the observed morphological

218   defects, with the appearance of distinct septal and off-septal PG foci appeared (marked with

219   HADA) in Δ*pbp1 tarO* and *pbp1*ΔPASTA *tarO* (Fig. 4 – figure supplement 1b-f), demonstrating

220   that both WTA and PBP1 are involved in cell cycle control in parallel.

221

222   As PBP1 PASTA has a role in the regulation of septal plate formation, this may be

223   determined by interacting with other protein components. In order to examine this hypothesis

224   we performed a bacterial two-hybrid assay, in which PBP1 has previously been found to have

225   multiple interactions (Steele et al., 2011). Truncation of the PASTA domains not only

226   reduced *S. aureus* PBP1 interaction with DivIB but also with FtsW, whilst recognition of

227   other known interacting partners of PBP1 (EzrA, PBP2 and DivIC) were unaffected by the

228   PASTA truncation (Fig. 5 – figure supplement 1a, b), suggesting that these wider interactions

229   involve the N-terminal domain of PBP1.

230

231   **PBP1 PASTA domains bind peptidoglycan**

232   Impaired interaction with DivIB could be one explanation for why cells depleted of PBP1

233   PASTA domains initiate irregular piecrusts and septation defects accrue as a consequence.

234   PASTA domains have long been associated with PG binding because of work performed

235   mainly on serine/threonine protein kinases (STPK) (Mir et al., 2011; Shah et al., 2008;

236   Squeglia et al., 2011; Yeats et al., 2002). Therefore, we assessed whether *S. aureus* PBP1 and

237   its PASTA domains could recognise PG by measuring their affinities for *S. aureus* cell wall

238   PG with or without WTA (+/-WTA) with a semi-quantitative fluorescence binding assay

239   (Bottomley et al., 2014) and *S. aureus* PBP1 derivatives produced in *Escherichia coli* (Fig. 5a

240   and Fig. 5 – figure supplement 1c). Both *Sa*PBP1 (K_d 19 ± 4 nM (+WTA), 115 ± 21 nM (-

241   WTA)) and its PASTA domains (*Sa*PASTA$_{PBP1}$; K_d 198 ± 42 nM (+WTA), 109 ± 23 nM (-

242   WTA) bound PG (Fig. 5b). Inactive SaPBP1* was still able to bind PG with a preference for

243   PG with WTA present (K_d 53 ± 8 nM (+WTA), 227 ± 46 nM (-WTA); Fig. 5b), similar to

244   active SaPBP1. Although removal of the PASTA domains did not abolish BocillinFL binding

245   (Fig. 5 – figure supplement 1c), it considerably reduced the ability of SaPBP1$_{\Delta PASTA}$ to bind

246   PG and binding was completely abolished in the presence of WTA (K_d >2000 nM (+WTA),

247   440 ± 57 nM (-WTA); Fig. 5b). By contrast, the PASTA domains (SaPASTA$_{PBP1}$) on their

248   own bind to $S. aureus$ PG but are incapable of binding BocillinFL (Fig. 5b and Fig. 5 – figure

249   supplement 1c). These results demonstrate unequivocally that PBP1 is a PG binding protein,

250   and the PASTA domains have a dominant role in this interaction. Sequence conservation

251   analysis of PASTA domains revealed the presence of either Arg or Glu residues in

252   classifying a PASTA domain as a PG-binder (Calvanese et al., 2017). The PASTA domains

253   of $S. aureus$ PBP1 each have proline at the equivalent positions (residues Pro603 and Pro661)

254   and thus PBP1 would be predicted as a non-PG binder, which clearly is not the case from the

255   experimental evidence presented herein. Not only have we demonstrated the existence of

256   such an interaction but we have also quantified it, suggesting that the predicted significance

257   of conserved Arg or Glu residues with regard to PG binding is either only relevant to PASTA

258   domains found in STPKs, linear arrangements of tandem PASTA repeats, or is too simplistic

259   a prediction for proteins with multiple and complex functions like PBPs.

260

261   To gain a better understanding of the role of the PASTA domains in $S. aureus$ PBP1

262   (SaPASTA$_{PBP1}$), we determined their structure by X-ray crystallography. Soluble

263   recombinant protein was obtained in high yield from the cytoplasm of $E. coli$ cells and well-

264   ordered crystals were subsequently produced that diffracted to a maximum resolution of 1.78

265   Å (Appendix Table 4). The structure was solved by molecular replacement using the

266   corresponding PASTA domains present in SpPBP2x from PDB entry 5OAU (Bernardo-

267　　García et al., 2018), which shares 26% sequence identity with SaPASTA$_{PBP1}$. The asymmetric

268　　unit contains two monomers (labelled A and B), each forming a 2-layer sandwich comprising

269　　an α-helix and a three-stranded antiparallel β-sheet, distinct from the TP domain (Fig. 5c).

270　　Clear and continuous electron density allowed the modelling and unambiguous assignment of

271　　both PASTA domains (Fig. 5c). When SaPASTA$_{PBP1}$ is compared with other structures

272　　deposited in the PDB using *DALI* (Holm, 2020), the top hit identified was *S. pneumoniae*

273　　PBP2x (Z-score; 15.7), showing a significant conservation of the PASTA fold, despite low

274　　sequence identity (Fig. 5c). Unlike the linear arrangement observed for PASTA domains in

275　　serine/threonine kinases (Barthe et al., 2010; Ruggiero et al., 2011), SaPASTA$_{PBP1}$ adopts a

276　　compact upside-down globular arrangement (Fig. 5c). The arrangement of the two PASTA

277　　domains solved here, in isolation from the TP domain in comparison to structural analyses of

278　　SpPBP2x, is entirely consistent with a non-linear PASTA domain arrangement. First, the

279　　structures of SaPASTA$_{PBP1}$ and the PASTA domains of SpPBP2x share a pairwise RMSD of

280　　2.2 Å over 114 Cα and when SaPASTA$_{PBP1}$ is superimposed on the PASTA domains of

281　　SpPBP2x there are no steric clashes with the TP domain. Second, the linker between PASTAs

282　　in SaPASTA$_{PBP1}$ has a sequence of DGDLTMPDMSGW, is neither glycine- nor alanine-rich,

283　　is not predicted to be disordered using IUPred2 or ANCHOR2 webservers and has a mean B

284　　factor of 44 Å^2 in comparison to a mean B factor of 42 Å^2 for the entire chain. Third, the

285　　interface between the PASTA domains is more reminiscent of the hydrophobic core of a

286　　globular protein than the more polar interface observed between molecules in crystal packing.

287　　It would therefore seem unlikely that the two PASTA domains open and close in a hinged

288　　manner, akin to the movement of a butterfly's wings, in the presence and absence of

289　　endogenous PG. Finally, the two proline residues that apparently define PBP1 as a non-binder

290　　of PG are found buried from solvent either at the interface of PASTA domain 1 with the TP

291　　domain (Pro603) or at the interface between the TP domain and PASTA domains 1 and 2

292   (Pro661). This latter interface includes the only tryptophan (Trp666) in the sequence of

293   *Sa*PASTA$_{PBP1}$; tryptophan residues are frequent 'markers' of carbohydrate binding sites in

294   proteins (Hudson et al., 2015) and in the absence of any obvious grooves or surface features

295   associated with conserved sequence distributions and/or electrostatics it remains unclear how

296   the PASTA domains of *Sa*PBP1 recognise PG.

297

298   **Discussion**

299   *S. aureus* has just two essential PBPs (Reed et al., 2015) and so forms an apparently simple

300   system to understand cell wall growth and division. Even the transpeptidase activity of these

301   two enzymes can be substituted by a single enzyme in the presence of β-lactam antibiotics

302   via the acquisition of PBP2A, encoded by *mecA*, in MRSA strains. Our recent study has

303   revealed that the presence of *mecA* and associated genetic lesions have a profound effect on

304   *S. aureus,* even in the absence of antibiotics (Panchal et al., 2020), leading to the discovery

305   herein that the PG biosynthetic activity of PBP1 is essential in MSSA but not in MRSA (Fig.

306   1d). This observation has important ramifications for many studies in *S. aureus* where the use

307   of an MRSA background can complicate phenotype interpretation. To understand the

308   fundamental role of PBP1 activity in basic cell physiology we have thus used a MSSA strain

309   with a defined genetic background.

310

311   The essential function of PBP1 is associated with its crucial role in septal PG synthesis

312   (Pereira et al., 2009; Reichmann et al., 2019). Here we show that PBP1 is a multifunction

313   regulatory and PG synthetic protein involved in both early and later stages of septum

314   synthesis. PBP1 can interact with other cell division components, make and bind to PG. PG

315   binding is primarily mediated by the PASTA domains that are essential for cell division.

316   There is clear overall structural similarity between *S. aureus* PBP1 and *S. pneumoniae* PBP2x

317   PASTA domains in the way that the two tandem PASTA domains associate into an anti-

318   parallel bundle (Fig. 5c); this is in marked contrast to the head-to-tail linear PASTA domain

319   repeats more typically found in STPKs. The highly hydrophobic interface between the two

320   PASTA domains means it is unlikely to open up like butterfly wings to bind to PG; similarly

321   an extensive, linear interaction with PG, which is likely to occur with the head-to-tail PASTA

322   domain arrangements seen in STPKs and that may require their dimerization (Barthe et al.,

323   2010), does not occur in *Sa*PBP1. Despite the successful production of diffracting crystals of

324   *Sa*PASTA$_{PBP1}$ grown in the presence of PG fragments (including an *N*-acetylglucosamine:*N*-

325   acetylmuramic acid disaccharide) none of the structures yielded electron density features

326   consistent with the stable binding of PG fragments. There are several potential explanations,

327   including a lack of affinity of PASTA domains for small PG fragments, unrepresentative of

328   the sacculus of *S. aureus*; our sedimentation assay does not permit the analysis of the binding

329   of PASTA domains to small, soluble PG precursors. Consequently, and in common with all

330   other PASTA domain structural analyses, the molecular details of PG recognition by *Sa*PBP1

331   remain elusive.

332

333   *S. aureus* is a spheroid coccus that can divide successively in three orthogonal planes

334   (Saraiva et al., 2020; Turner et al., 2010). Septation is first observed as the formation of a

335   thick band of PG known as the piecrust (Turner et al., 2010). This then transitions to the

336   production of the septal plate itself, an initially V-shaped structure with a narrower leading

337   edge (Lund et al., 2018). After closure of the septal annulus, the now bowed septum fills out

338   to yield the mature structure prior to septal scission. The septal plate has two distinct PG

339   architectures with a ring-like pattern at its core, which is exposed upon scission, and a

340   subsequently-synthesised fine mesh, akin to the rest of the peripheral cell wall (Pasquina-

341   Lemonche et al., 2020). Loss of the entire PBP1, or just its PASTA domains, does not

342 prevent piecrust formation but does result in multi- and/or off-centre piecrusts without the

343 ability to produce the septal plate (Fig 2f). Thus, piecrust formation does not require PBP1

344 but is likely the result of the activity of the essential PBP2. PBP1 may regulate division site

345 selection through PG cell wall recognition via its PASTA domains. Alternatively, as the

346 division apparatus is unable to progress effectively to septal plate formation due to the lack of

347 PBP1, this may lead to further rounds of initiation and piecrust formation. PBP1 has a clear

348 role in septal plate formation where in the absence of PBP1 or the PASTA domains, cells

349 form aberrantly shaped septa that do not close their annuli (Fig. 2a-e). In stark contrast,

350 inactivation of PBP1 TP activity (*pbp1**) does not stop inward septum progression as

351 observed with loss of PBP1 or the PASTA domains, however, such septa are mis-shapen,

352 curved and abnormally thick (Fig. 2a-e and Fig. 3). The use of the PBP1-specific antibiotic

353 MEM at 1x MIC led to the similar morphology of thickened and mis-shapen septa. Two

354 independent avenues of research both lead to the conclusion that PBP1 TP activity is

355 essential and, whilst septum formation is disturbed, it is not entirely prevented. Therefore

356 PBP1 retains its regulatory function(s) regardless of activity loss. As well as binding to the

357 cell wall, PBP1 also interacts with multiple protein partners including EzrA, DivIB/C, PBP2

358 and FtsW (Fig. 5 – figure supplement 1a, b) (Steele et al., 2011; Reichmann et al., 2019).

359 Recently, the PASTA domains from *B. subtilis* PBP2B were shown to regulate PBP2B

360 interaction with DivIB (Morales Angeles et al., 2020). *S. aureus* DivIB is a PG binding

361 protein essential for division, which depletion leads to septal plate formation loss (Bottomley

362 et al., 2014; Steele et al., 2011)`. Here the PBP1 PASTA domains were found to bind DivIB

363 and FtsW, alluding to their essential role in cell division. FtsW is a SEDS protein, whose TG

364 activity requires the presence of PBP1 (Taguchi et al., 2019). Bifunctional aPBPs (including

365 PBP2) and bPBP-SEDS (including PBP1-FtsW) pairs share similar activities but the fact they

366 coexist in many bacterial species implies there is a division of responsibilities between them.

367 Indeed, it has been proposed lately that bPBP-SEDS pairs likely lay the primary PG matrix,

368 while aPBPs support the initial PG by modifying, filling in and adding PG to it (Cho et al.,

369 2016; Straume et al., 2020). The *S. aureus* septal plate PG has two distinct architectures, a

370 disordered mesh present on its cytoplasm facing side and a ring structure at its core, which is

371 revealed after the cells have split (Pasquina-Lemonche et al., 2020; Turner et al., 2010) (Fig.

372 5 – figure supplement 2). Recent AFM analysis from *Staphylococcus warneri* also describes

373 the distinct PG architectures during septation as piecrust and septal plate rings/mesh (Su et

374 al., 2020) . When sacculi are purified from *S. warneri*, the septum can split apart revealing

375 the rings, even in septa that have not closed their annulus, showing that the rings are not a

376 result of PG hydrolysis during cell scission. We hypothesise (Fig. 5 – figure supplement 2)

377 that once the piecrust has been produced, PBP1 and FtsW use this as a foundation to initiate

378 septal plate formation. Together they make the rings of material that become the core of the

379 developing septum, providing the framework for PBP2 to make the bulk of the septal plate as

380 a tight mesh alongside PBP4 and the insertion of WTA via the *tar* pathway. Loss of PBP1 TP

381 activity in the presence of active PBP2 leads to the lack of the ring framework and aberrant,

382 unproductive septum formation. The rings that form the centre of the developing septum also

383 provide the cleavage plane during scission.

384

385 Cell division is a fundamental requirement for life. A central question to this in bacteria is how

386 is the division septum synthesised and then split to yield two daughter cells whilst maintaining

387 cellular integrity in the face of internal turgor? Here we have begun to answer this question by

388 revealing the complex synthesis coordination mechanisms that allow this biological

389 engineering feat to be accomplished.

16

Materials and methods

Bacterial growth conditions

Strains used in this study are listed in Appendix Table 1.

All *Staphylococcus aureus* strains were grown in tryptic soy broth (TSB) containing

appropriate antibiotics at 37°C, unless otherwise indicated, with aeration.

All *Escherichia coli* strains, unless otherwise stated, were grown in Lysogeny broth (LB)

containing appropriate antibiotics at temperatures ranging from 20°C to 37°C with aeration.

For solid media 1.5% (w/v) agar was added.

When necessary, growth medium was supplemented with kanamycin (50 μg ml^{-1}),

tetracycline (1 μg ml^{-1}), chloramphenicol (10 μg ml^{-1}, *S. aureus*; 30 μg ml^{-1}, *E. coli*),

erythromycin (5 μg ml^{-1}), spectinomycin (250 μg ml ml^{-1}), ampicillin (100 μg ml^{-1}),

meropenem (0.4 μg ml^{-1}, 1x MIC for SH1000 WT; 0.2 μg ml^{-1}, 1x MIC for *pbp3 pbp4*), 5-

bromo-4-chloro-3-indolyl β-d-thiogalactopyranoside (X-Gal; 80 μg ml^{-1}, *S. aureus*;

40 μg ml^{-1}, *E. coli*) or isopropyl β-d-thiogalactopyranoside (IPTG, 50 μM or 1 mM).

Plasmid construction

Plasmids and oligos used in this study are listed in Appendix Table 2 and Appendix Table 3,

respectively.

Plasmids were cloned using *E. coli* NEB5α following previously described methods (Gibson

et al., 2009; Sambrook et al., 1989).

pKB-P*spac*-*pbp1*

A fragment containing RBS and coding region of *S. aureus pbp1* was PCR amplified from

the genomic DNA of *S. aureus* SH1000 using pCQ-pbp1-F/-R primers and cloned into NheI

and AscI cut pCQ11-FtsZ-SNAP by Gibson assembly, resulting in pCQ11-P*spac*-*pbp1*. Next

17

415   the region containing P*spac*, RBS and *pbp1* was PCR amplified from pCQ11-P*spac-pbp1*

416   using pKB-Pspac-pbp1-F/-R primers and cloned into BamHI and EcoRI cut pKASBAR by

417   Gibson assembly giving pKB-P*spac-pbp1*.

418

419   **pMAD-Δ*pbp1***

420   Fragments encompassing 1 kb regions flanking upstream (from -980 bp upstream of *pbp1* to

421   first 20 bp of *pbp1*) and downstream of (from 2214 bp of *pbp1* to 970 bp downstream of

422   *pbp1*) *pbp1* were PCR amplified from *S. aureus* SH1000 genomic DNA using primer pairs

423   pbp1-A/-B and pbp1-C/-D, respectively, and cloned into BamHI and EcoRI cut pMAD by

424   Gibson assembly, creating a deletion vector pMAD-Δ*pbp1*.

425

426   **pMAD-*pbp1*$_{\Delta PASTA}$**

427   Fragments encompassing 1.5 kb regions flanking the region encoding *pbp1* PASTA domains

428   (upstream, from 286 bp to 1785 bp of *pbp1*; downstream, from 2214 bp of *pbp1* to 970 bp

429   downstream of *pbp1*) were PCR amplified from *S. aureus* SH1000 genomic DNA using

430   pbp1-E/-F and pbp1-G/-H primers and cloned into BamHI and EcoRI cut pMAD by Gibson

431   assembly, resulting in a deletion vector pMAD-*pbp1*$_{\Delta PASTA}$.

432

433   **pMAD-*pbp1****

434   A ~1.3 kb fragment covering an upstream region of the active site of *pbp1* (from -334 bp

435   upstream of *pbp1* to first 950 bp of the *pbp1* coding sequence), and a ~1.3 kb fragment

436   comprising the 3′ fragment of *pbp1* (930-2235 bp region of *pbp1*) were PCR amplified from

437   *S. aureus* SH1000 genomic DNA using primer pairs pbp1*5′-F/-R and pbp1*3′-F/-R,

438   respectively. Primers pbp1*5′-R and pbp1*3′-F were designed to introduce a T to G point

439   mutation resulting in a Ser314Ala substitution. The PCR products were ligated with pMAD

440   cut with EcoRI and BamHI by Gibson assembly, resulting in pMAD-*pbp1**.

441

442   **T25-PBP1$_{\Delta PASTA}$**

443   A fragment encoding *S. aureus pbp1* without the PASTA domains (M1-S595) was PCR

444   amplified from *S. aureus* SH1000 genomic DNA using T25-pbp1-F and T25-pbp1pasta-R

445   and cloned into BamHI and EcoRI cut pKT25, resulting in T25-PBP1$_{\Delta PASTA}$.

446

447   **pVR plasmids**

448   Full-length *pbp1* (M1-D744) was *E. coli* codon optimised, synthesised by GenScript, PCR

449   amplified using VR47F/R and cloned into KpnI and HindIII cut pOPINRSF using In-Fusion

450   cloning (Takara Bio), resulting in pVR01. Construction of pVR02 (*Sa*PBP1, M37-D744) and

451   pVR06 (*Sa*PASTA$_{PBP1}$, S595-D744) was performed using inverse PCR (iPCR) (Erster &

452   Liscovitch, 2010), pVR01 as a template and primer pairs VR49F/VR49R and

453   VR57F/VR49R, respectively. pVR03 (*Sa*PBP1*, M37-D744, S314A) and pVR04

454   (*Sa*PBP1$_{\Delta PASTA}$, M37-S595), were constructed by QuikChange Site-Directed Mutagenesis of

455   pVR02 using VR51 and VR53, respectively.

456

457   **pSA50**

458   In order to construct an overexpression plasmid for sPBP1-BAP, A51-D744 fragment of *E.*

459   *coli* codon optimised *pbp1* was PCR amplified using primers OPPF20018F/OPPF20018R

460   and cloned into KpnI and SfoI cut pOPINJB by In-Fusion cloning (Takara Bio). The resulting

461   construct, pSA50 contains an N-terminal hexahistidine-tag fused to Glutathione-S-transferase

462   followed by a Human Rhinovirus 3C protease site, while the PBP1 (A51-D744) C-terminal

463   end is fused to a Biotin Acceptor Peptide (BAP) sequence.

19

464

Construction of *S. aureus* mutants

465

466 All vectors were passed through a restriction-deficient *S. aureus* RN4220 before being

467 transduced into a final *S. aureus* SH1000 strain. Transformation and phage transduction of *S.*

468 *aureus* were carried out as described previously (Novick & Morse, 1967; Schenk & Laddaga,

469 1992).

470

471 **Δ*pbp1*, *pbp1*ΔPASTA and *pbp1****

472 For construction of *pbp1* mutation strains, first an ectopic copy of *pbp1* under the control of

473 the P*spac* promoter was introduced at the lipase (*geh*) locus. Electrocompetent CYL316 was

474 transformed with pKB-P*spac-pbp1*. The chromosomal fragment containing the integrated

475 plasmid was moved into *S. aureus* SH1000 by phage transduction, resulting in SJF4588 (*S.*

476 *aureus* SH1000 *geh::Pspac-pbp1*). Next electrocompetent RN4220 was transformed with

477 pMAD-Δ*pbp1*, pMAD-*pbp1*ΔPASTA or pMAD-*pbp1** and the plasmids were moved to

478 SJF4588 by phage transduction. Integration at 42°C and excision at 28°C of pMAD-Δ*pbp1*,

479 pMAD-*pbp1*ΔPASTA or pMAD-*pbp1**, resulted in strains SJF5116, SJF5275 and SJF4590,

480 respectively. To allow controlled expression of *pbp1* from P*spac*, pGL485, a multi-copy

481 plasmid carrying *lacI*, was introduced creating strains Δ*pbp1* (*S. aureus* SH1000 *geh::Pspac-*

482 *pbp1* Δ*pbp1 lacI*), *pbp1*ΔPASTA (*S. aureus* SH1000 *geh::Pspac-pbp1 pbp1*ΔPASTA *lacI*) and

483 *pbp1** (*S. aureus* SH1000 *geh::Pspac-pbp1 pbp1** *lacI*).

484

485 **MRSA Δ*pbp1* and MRSA *pbp1****

486 In order to construct high-level β-lactam resistant mutants, Δ*pbp1* and *pbp1** were

487 transformed with a phage lysate from SJF5046 (*S. aureus* SH1000*lysA::pmecA rpoB*[H929Q])

488 with selection for erythromycin resistance, resulting in low-level β-lactam resistant Δ*pbp1*

20

489   p*mecA* and *pbp1** p*mecA*. The low-level resistant mutants were transduced again with the

490   phage lysate from SJF5046 and selected for kanamycin resistance, resulting in MRSA Δ*pbp1*

491   (*S. aureus* SH1000 *geh::Pspac-pbp1 Δpbp1 lacI lysA::*p*mecA rpoB*^{H929Q}) and MRSA *pbp1**

492   *pbp1* (*S. aureus* SH1000 *geh::Pspac-pbp1 pbp1* lacI lysA::*p*mecA rpoB*^{H929Q}). MIC values

493   were determined using antibiotic susceptibility tests using E-test M.I.C. Evaluator (Oxoid)

494   strips.

495

496   **pbp3 pbp4**

497   SH1000 was transduced with a phage lysate from NE420 (*S. aureus* JE2 *pbp3::Tn*) resulting

498   in SH4421 (*S. aureus* SH1000 *pbp3::Tn*). To swap the erythromycin resistance cassette to a

499   kanamycin cassette, SH4425 (*S. aureus* SH1000 *pbp4::Tn*) was transduced with a phage

500   lysate from NE3004 (*S. aureus* RN4220 pKAN). Integration at 42°C and excision at 28°C of

501   pSPC resulted in strain SH5115 (*S. aureus* SH1000 *pbp4::kan*). SH4421 was subsequently

502   transduced with a phage lysate from SH5115 (*S. aureus* SH1000 *pbp4::Tn*) resulting in *pbp3*

503   *pbp4* (SH5483; *S. aureus* SH1000 *pbp3::Tn pbp4::kan*).

504

505   **Δ*pbp1* *pbp4*, *pbp1*ₐₚₐₛₜₐ *pbp4* and *pbp1* pbp4***

506   Δ*pbp1*, *pbp1*ₐₚₐₛₜₐ and *pbp1** were transduced with a phage lysate from SH5115 (*S. aureus*

507   SH1000 *pbp4::kan*), resulting in Δ*pbp1 pbp4* (*S. aureus* SH1000 *geh::Pspac-pbp1 Δpbp1*

508   *lacI pbp4::kan*), *pbp1*ₐₚₐₛₜₐ *pbp4* (*S. aureus* SH1000 *geh::Pspac-pbp1 pbp1*ₐₚₐₛₜₐ *lacI*

509   *pbp4::kan*) and *pbp1* pbp4* (*S. aureus* SH1000 *geh::Pspac-pbp1 pbp1* lacI pbp4::kan*),

510   respectively.

511

512   **pbp1* pbp3 pbp4**

21

513   *pbp1* pbp4* (*S. aureus* SH1000 *geh::Pspac-pbp1 pbp1* lacI pbp4::kan*) was transduced with

514   a phage lysate from SH4421 (*S. aureus* SH1000 *pbp3::Tn*), resulting in *pbp1* pbp3 pbp4* (*S.*

515   *aureus* SH1000 *geh::Pspac-pbp1 pbp1* lacI pbp3::Tn pbp4::kan*)**.**

516

Δ*pbp1 ezrA-gfp*, *pbp1*$_{\Delta PASTA}$ *ezrA-gfp* and *pbp1* ezrA-gfp*

518   Δ*pbp1*, *pbp1*$_{\Delta PASTA}$ and *pbp1** were transduced with a phage lysate from JGL227 (*S. aureus*

519   SH1000 *ezrA-gfp+*), resulting in Δ*pbp1 ezrA-gfp* (*S. aureus* SH1000 *geh::Pspac-pbp1* Δ*pbp1*

520   *lacI ezrA-gfp*)*, pbp1*$_{\Delta PASTA}$ *ezrA-gfp* $_{PASTA}$ (*S. aureus* SH1000 *geh::Pspac-pbp1 pbp1*$_{\Delta PASTA}$

521   *lacI ezrA-gfp*) and *pbp1* ezrA-gfp* (*S. aureus* SH1000 *geh::Pspac-pbp1 pbp1* lacI ezrA-gfp*)*,*

522   respectively**.**

523

Δ*pbp1 tarO*, *pbp1*$_{\Delta PASTA}$ *tarO* and *pbp1* tarO*

525   Δ*pbp1*, *pbp1*$_{\Delta PASTA}$ and *pbp1** were transduced with a phage lysate from *tarO tarO+* (*S.*

526   *aureus* SA113 Δ*tarO::ery* pUC1-*tarO*), resulting in Δ*pbp1 tarO* (*S. aureus* SH1000

527   *geh::Pspac-pbp1* Δ*pbp1 lacI* Δ*tarO::ery*)*, pbp1*$_{\Delta PASTA}$ *tarO* $_{PASTA}$ (*S. aureus* SH1000

528   *geh::Pspac-pbp1 pbp1*$_{\Delta PASTA}$ *lacI* Δ*tarO::ery*) and *pbp1* tarO* (*S. aureus* SH1000

529   *geh::Pspac-pbp1 pbp1* lacI* Δ*tarO::ery*)*,* respectively**.**

530

PBP1 depletion

532   P*spac-pbp1* strains were grown from an OD_{600} of 0.1 to exponential phase ($OD_{600} \sim 0.5$) in

533   TSB containing 10 µg ml^{-1} chloramphenicol and 50 µM IPTG. Cells were washed three

534   times by centrifugation and resuspension in TSB. Washed cells were then used to inoculate

535   TSB 10 µg ml^{-1} chloramphenicol. Cultures were inoculated to an OD_{600} 0.05 for phenotypic

536   studies and an OD_{600} 0.005 for growth studies. For phenotypic analysis, cultures were

537   incubated for 2 h to allow depletion of PBP1 before microscopy imaging. Control samples

22

538   were grown in TSB supplemented with 10 µg ml^{-1} chloramphenicol and 1 mM (50 µM, *ezrA-*

539   *gfp* mutants) IPTG.

540   For the plating efficiency test, cells grown in the presence of 10 µg ml^{-1} chloramphenicol and

541   50 µM IPTG to exponential phase (OD$_{600}$ ~ 0.5) were washed three times in PBS. Serial

542   dilutions of washed cells were plated on TSB 10 µg ml^{-1} chloramphenicol with or without 1

543   mM IPTG. Relative plating efficiency ($\%CFU$) is expressed as the number of cells that grow

544   on plates without IPTG ($CFU_{no\ IPTG}$) to cells that grow in the presence of IPTG (CFU_{IPTG})

545   multiplied by 100%:

546
$$\%CFU = \frac{CFU_{no\ IPTG}}{CFU_{IPTG}} \times 100\%$$

547

548   **Meropenem activity assays**

549   *S. aureus* strains were grown overnight in TSB. The overnight cultures were used to inoculate

550   fresh TSB media to an OD$_{600}$ of 0.05. When cells reached an OD$_{600}$ of 0.2-0.4, meropenem

551   was added, and the change of bacterial count was monitored. The colony-forming units per

552   ml of culture (CFU/ml) measures were normalized to the initial CFU/ml at the time of the

553   antibiotic addition, at time zero (*t$_0$*).

554
$$Relative\ CFU/ml = \frac{CFU/ml_{tn}}{CFU/ml_{t0}}$$

555   For phenotypic analysis, cells were treated for 1 h with 1x MIC meropenem before

556   microscopy imaging.

557

558   **Fractionation of *S. aureus* membranes**

559   The membrane fraction of *S. aureus* was prepared as previously described (García-Lara et al.,

560   2015) with the following modifications. *S. aureus* cells grown to the appropriate growth

561   phase were recovered by centrifugation (5,000 x g, 10 min, 4°C), washed three times by

562 resuspension and centrifugation (5,000 x g, 10 min, 4°C) in PBS. Cells were resuspended in

563 TBSI and broken using 0.1 mm silica spheres (Lysing Matrix B) and FastPrep Homogenizer

564 (MP Biomedicals) in 12 cycles of 30 s, at maximum speed (6.5 m s^{-1}), with 5 min incubation

565 on ice between cycles. Cell lysates were centrifuged (5,000 x g, 10 min, 4°C) to remove

566 unbroken cells. The supernatant was then spun (5,000 x g, 10 min, 4°C) to sediment cell wall

567 material. The membrane fraction was recovered from the supernatant by centrifugation

568 (35,000 x g, 20 min, 4°C) and the pellet (membranes) was resuspended in PBS. The total

569 protein concentration was estimated by Bradford assay.

570

571 ***In vitro* labelling of *S. aureus* PBPs with BocillinFL**

572 This method was adopted from a published protocol (Zhao et al., 1999) with minor

573 modifications. Membrane proteome samples (25 μg in 20 μl PBS) and purified proteins (2.5

574 μg in 25 μl HEPES pH 7.5 150 mM NaCl) were incubated with 25 μM BocillinFL

575 (Invitrogen) for 20 min at 37°C. Additionally for competition assay, purified *Sa*PBP1 was

576 mixed with 2.5 μg (~286 μM final concentration) ampicillin and incubated at 37˚C for 10

577 min prior to the addition of BocillinFL. The reaction was stopped by the addition of 5x SDS-

578 PAGE loading buffer. Membrane proteome was additionally incubated for 10 min at 90°C.

579 The samples were run on a 6-20% (w/v) SDS-PAGE gradient or 10% (w/v) SDS-PAGE gel

580 and visualized using a BioRad ChemiDoc MP Imaging system or a GE Typhoon FLA 9500.

581

582 **Labelling *S. aureus* DAAs**

583 *S. aureus* cells were incubated with 500 μM (2 mM for *pbp4* mutants) HADA or 1 mM

584 ADA-DA at 37°C for 5 min. Cells were then washed by centrifugation and resuspension in

585 PBS.

586

Click chemistry

587

588 ADA-DA containing an azide functional group was fluorescently labelled with Alexa Fluor

589 488 Alkyne at 5 µg ml^{-1} via the Click reaction (copper (I)-catalysed alkyne-azide

590 cycloaddition). This was carried out using the Click-iT Cell Reaction Buffer Kit

591 (ThermoFisher) according to the manufacturer's protocol.

592

593 **Labelling *S. aureus* with fluorescent NHS-ester**

594 Fixed cells wells were resuspended in PBS containing 8 µg ml^{-1} Alexa Fluor 555 NHS ester

595 (Invitrogen) and incubated at room temperature for 30 min. Cells were washed twice by

596 centrifugation and resuspension in PBS.

597

598 **Fixing for fluorescence microscopy**

599 Cells were fixed by incubation in 1.6% (w/v) paraformaldehyde at room temperature for 30

600 min.

601

602 **Fluorescence microscopy**

603 Fixed cells were dried onto a poly-l-Lysine coated slide, mounted in PBPS and imaged on a

604 Nikon Ti Inverted microscope fitted with a Lumencor Spectra X light engine. Images were

605 taken using a 100x PlanApo (1.4 NA) oil objective using 1.518 RI oil and detected by an

606 Andor Zyla sCMOS camera.

607

608 **Cell volume estimation**

609 Cell volume calculations were carried out as previously described (Zhou et al., 2015). The

610 long and short axis of cells were measured using Fiji. The volume was then calculated based

611 on a prolate spheroid shape with volume:

612
$$V = \frac{4}{3}\pi ab^2,$$

613 where *a* and *b* are the radii along the long and short axis, respectively.

614

Transmission electron microscopy

616 *S. aureus* strains were prepared for electron microscopy as previously described (Sutton et

617 al., 2021).

618

Preparation of *S. aureus* sacculi

620 Peptidoglycan from *S. aureus* cells was extracted and if required HF treated to remove cell

621 wall polymers as previously described (Sutton et al., 2021).

622

Sacculi immobilisation for AFM Imaging

624 Immobilisation surface was prepared by adding the solution mixed by 171 μL 100 mM

625 NaHCO$_3$, 3 μl of 1 M NaOH and 6 μl of Cell-Tak (Corning, 5% (w/v) in acetic acid) on

626 freshly cleaved mica. After 30 min incubation, the surface was washed by 5 × 200 μl HPLC

627 grade water. Sacculi stocks were 10 times diluted in HPLC grade water and briefly tip-

628 sonicated to re-suspend in prior to immobilisation. 10 μl of the sacculi suspension was added

629 to 40 μl of HPLC grade water on the Cell-Tak immobilisation surface and incubated for 1 h.

630 The surface was then thoroughly rinsed with HPLC grade water, blow-dried with nitrogen

631 and stored in petri-dish at room temperature before AFM imaging.

632

AFM Imaging and image analysis

634 AFM imaging was carried out on a Nanowizard III ULTRA Speed system (JPK, Germany).

635 Rectangular cantilevers with nominal spring constant of 0.3 N/m and resonant frequency (in

636 liquid) of ~ 150 kHz (USC-F0.3-k0.3, NanoWorld, Switzerland) were used. The spring

637   constant and deflection sensitivity of each cantilever was calibrated prior to each

638   measurement (Hutter & Bechhoefer, 1993; Sader et al., 2016) Measurements were carried out

639   in Quantitative Imaging mode at room temperature, in the buffer composed of 200 mM KCl

640   and 10 mM Tris. Scans were driven at a line rate of ~ 0.78 Hz, with a typical Z length of 300

641   nm and trigger force of 20 nN.

642   Resultant topographic images were processed using JPK Data Processing. No flattening or

643   surface subtraction was applied. High pass filter (scale: 100% to 500%, degree of smoothing:

644   5 px, horizontal) was applied to the higher magnification images to enhance the contrast

645   without modifying the morphological features. The morphological features of sacculi were

646   summarised from images obtained on abundant technical repeats of 2 biological replicates.

647

648   **Recombinant protein production and purification**

649   **sPBP1-BAP**

650   *E. coli* BL21(DE3) cells containing plasmid pSA50 were grown in LB medium supplemented

651   with 100 μg ml^{-1} ampicillin at 37°C to an OD$_{578}$ of 0.5. Protein overproduction was induced

652   by addition of 0.5 mM IPTG to the cell culture and further incubation for 4 h at 30°C. Cells

653   were harvested by centrifugation (6,200 x g, 15 min, 4°C) and the pellet was resuspended in

654   basic buffer (25 mM Tris-HCl, 100 mM NaCl, pH 7.5). After addition of 1 mM PMSF,

655   1:1,000 dilution of protease inhibitor cocktail (Sigma-Aldrich) and DNase, the cells were

656   disrupted by sonication (Branson Digital Sonifier). The cell lysate was centrifuged (130,000

657   x g, 60 min, 4°C) and the supernatant was recovered. The supernatant was incubated with Ni-

658   NTA Superflow (Qiagen) for 2 h at 4°C with gentle stirring, which had been pre-equilibrated

659   in basic buffer. The resin was poured into a gravity column and washed with 20 volumes of

660   wash buffer (25 mM Tris-HCl, 150 mM NaCl, 10% (v/v) glycerol, 10 mM MgCl$_2$, 20 mM

661   imidazole, pH 7.5). Bound protein was eluted with elution buffer (25 mM Tris-HCl, 150 mM

662   NaCl, 10% (v/v) glycerol, 10 mM MgCl$_2$, 600 mM imidazole, pH 7.5). 10 U ml^{-1} of HRV-

663   3C protease (Takara) were added to the Ni-NTA eluted protein to remove the oligohistidine-

664   GST-tag during dialysis against 3 L of dialysis buffer I (25 mM Tris-HCl, 150 mM NaCl, 10

665   mM EGTA, 10% (v/v) glycerol, pH 7.5) for 20 h at 4°C. Digested protein was dialysed

666   against 3 L of dialysis buffer II (25 mM Tris-HCl, 150 mM NaCl, 10 mM MgCl$_2$, 10% (v/v)

667   glycerol, pH 7.5), for 3 h at 4°C. The protein was incubated in the same Ni-NTA beads (pre-

668   equilibrated in dialysis buffer II) for 2 h at 4°C to remove the contaminants and the His-GST

669   tag from the sample. The flow through and the washes (2 volume of wash buffer) were

670   pooled, dialysed against storage buffer (25 mM HEPES-NaOH, 150 mM NaCl, 10 mM

671   MgCl$_2$, 10% (v/v) glycerol, pH 7.5) and concentrated using a Vivaspin Turbo 15 column

672   (MWCO 50000 Da).

673

674   ***Sa*PBP1, *Sa*PBP1*, *Sa*PBP1$_{\Delta PASTA}$ and *Sa*PASTA$_{PBP1}$**

675   All recombinant proteins were produced in *E. coli* Rosetta (DE3) cells at 37°C in TB medium

676   supplemented with 50 µg ml^{-1} kanamycin and 30 µg ml^{-1} chloramphenicol. Once cultures had

677   reached OD$_{600}$ 0.9, protein expression was induced with 1 mM IPTG for 20 h at 20°C. Cells

678   were harvested by centrifugation (4,000 x g at 4°C for 30 mins) and the pellet was

679   resuspended in a buffer of 50 mM Tris-HCl pH 8.0, 500 mM NaCl, 20 mM imidazole

680   supplemented with one EDTA-free protease inhibitor cocktail tablet (Roche) and DNAse (4

681   µg ml^{-1} final concentration). Cells in this resuspension were lysed by two passes through a

682   One-Shot cell disruptor (Constant Systems) at 23 kpsi and the cell debris was removed by

683   centrifugation (40,000 x g at 4°C for 30 min). The first purification step was affinity

684   chromatography with a 5 mL HisTrap™ FF column (GE Healthcare) precharged with Ni^{2+}

685   and equilibrated in buffer A (50 mM Tris-HCl, pH 8.0, 500 mM NaCl, 20 mM imidazole). A

686   linear concentration gradient of imidazole was applied to elute the protein using buffer B (50

687   mM Tris-HCl, pH 8.0, 500 mM NaCl, 800 mM imidazole). Further purification was carried

688   out by size exclusion chromatography using a Superdex™ 200 Hi Load 16/60 column (GE

689   Healthcare). Proteins were eluted with SEC buffer (25 mM Tris-HCl, pH 8.0, 150mM NaCl)

690   and analysed by SDS-PAGE.

691

692   **Generation of anti-PBP1 antibody**

693   Serum against sPBP1A-BAP was produced from rabbits following a 28-day immunisation

694   program at Eurogentec (Belgium), and it was purified as previously described (Bertsche et

695   al., 2006).

696

697   **Immunoblot analysis**

698   *S. aureus* cultures were washed three times by resuspension and centrifugation (5,000 x g, 10

699   min, 4°C) in PBS. Cells were resuspended in TBSI (50 mM Tris, 100 mM NaCl, pH 8, plus

700   Complete Protease Inhibitor Cocktail, Roche) and broken using 0.1 mm silica spheres

701   (Lysing Matrix B) and FastPrep Homogenizer (MP Biomedicals) in 12 cycles of 30 s, at

702   maximum speed (6.5 m s^{-1}), with 5 min incubation on ice between cycles. Cell lysates were

703   centrifuged (5,000 x g, 10 min, 4°C) to remove unbroken cells. ~ 60 μg of total protein was

704   separated on a 12% (w/v) SDS-PAGE gel and electroblotted onto a nitrocellulose membrane

705   and blocked in 5% (w/v) skimmed-milk in TBST (20 mM Tris-HCl, pH 7.6; 17 mM NaCl,

706   0.1% (v/v) Tween-20). The membrane blocked in 5% (w/v) skimmed-milk in TBST (20 mM

707   Tris-HCl, pH 7.6; 17 mM NaCl, 0.1% (v/v) Tween-20) was incubated with primary

708   polyclonal anti-PBP1 (1:1,000) overnight with gentle agitation at 4°C. Primary antibodies

709   were detected using horseradish peroxidase-conjugated goat anti-rabbit IgG (1:10,000,

710   BioRad) and Clarity Western ECL Substrate (BioRad) reagent according to the

29

711 manufacturer's protocol. Chemiluminescence was detected using Syngene G:BOX Chemi

712 XX9.

713

714 **Crystallisation, data collection and structure determination**

715 Crystallisation of SaPASTA$_{PBP1}$ was carried out at 20°C by the sitting-drop vapour diffusion

716 method in 96-well MRC plates (Molecular Dimensions) with a Mosquito crystallisation robot

717 (TTP LabTech) and commercial crystallisation screens (Hampton Research and Molecular

718 Dimensions). Orthorhombic crystals of diffraction quality, with a maximum dimension of

719 approximately 500 μm, appeared overnight from a mixture of equal volumes of protein

720 solution (42 mg ml^{-1} in 25 mM Tris-HCl, pH 8.0, 150 mM NaCl) and reservoir solution (0.2

721 M NaCl, 0.1 M sodium/potassium phosphate pH 6.2, 50 % (v/v) PEG 200). Diffraction data

722 were indexed and integrated using XDS (Kabsch, 2010) and scaled using AIMLESS (Evans

723 & Murshudov, 2013) from the CCP4 program suite (Winn et al., 2011). The crystals display

724 space group $P2_12_12_1$ with unit cell lengths a = 39.8 Å, b = 81.4 Å and c = 89.6 Å. The

725 asymmetric unit consists of two polypeptide chains with an estimated solvent content of 45 %

726 and a V$_m$ of 2.24 Å^3/Da. The region corresponding to the two PASTA domains in the crystal

727 structure of *S. pneumoniae* PBP2x (PBP 5OAU) was used as a molecular replacement search

728 model, sharing approximately 26 % sequence identity with SaPASTA$_{PBP1}$. The search model

729 was generated using phenix.sculptor (Bunkóczi & Read, 2011) to remove non-

730 macromolecular chains and prune sidechains. The structure was solved by molecular

731 replacement using PHASER (McCoy et al., 2007) and the resultant electron density map was

732 of high quality, allowing the tracing of the main chain. Model building and refinement were

733 carried out with Coot (Emsley et al., 2010) and Phenix (Liebschner et al., 2019), respectively.

734 Assessments of the geometry and validation of the final model was carried out using

735 Molprobity (Chen et al., 2010). Analyses of surface areas and interactions were made using

736   the PISA web service (Krissinel & Henrick, 2007). The graphics program PyMOL

737   (Schrödinger, LLC, 2015) was used to generate all molecular figures presented.

738

739   **Cell wall binding assays**

740   Cell wall binding assays of recombinant PBP1 proteins fluorescently labelled with Cy2 bis-

741   reactive dye (GE Healthcare) were performed as previously described (Bottomley et al.,

742   2014).

743

744   **Bacterial two-hybrid**

745   Competent BTH101 was co-transformed with pKT25 and pUT18 derivatives. Transformants

746   were selected on LB agar plates containing 100 μg ml^{-1} ampicillin, 50 μg ml^{-1} kanamycin

747   and 40 μg ml^{-1} X-Gal and incubated at 30°C. Single colonies were grown in 150 μl LB with

748   100 μg ml^{-1} ampicillin, 50 μg ml^{-1} kanamycin and 0.5 mM IPTG at 30°C.

749   To qualitatively measure for pairwise interactions, 5 μl of each overnight culture were spotted

750   onto LB agar plates containing 100 μg ml^{-1} ampicillin, 50 μg ml^{-1} kanamycin, 0.5 mM IPTG

751   and 40 μg ml^{-1} X-Gal. Plates were incubated at 30°C 24 – 48 h in an environment protected

752   from light and imaged. To quantify interactions, overnight cultures were assayed for β-

753   galactosidase activity against MUG (4-methylumbelliferyl-β-d-galactopyranoside) using an

754   assay as previously described (Steele et al., 2011).
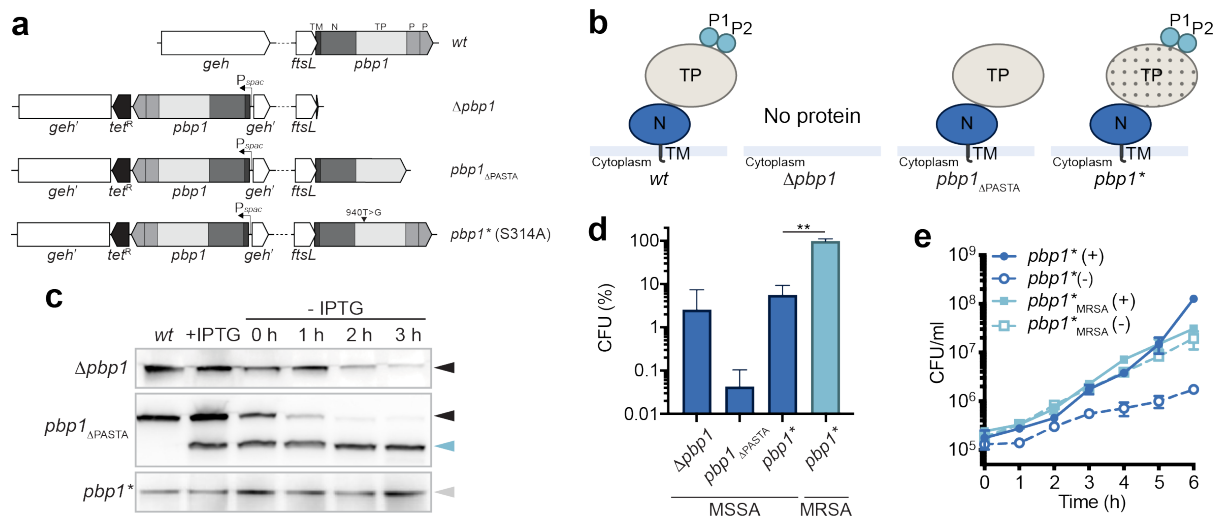
755

756   **Acknowledgements**

764

Competing Interests

766   The authors declare no competing interests.

767 **Figures and figure legends**

768

769

770 **Fig. 1 Essentiality of PBP1**

771 **a**, Schematic representation of genetic constructs used in this study. In *S. aureus* WT (*wt*) the

772 5′ end of *pbp1* overlaps with the 3′ of *ftsL*. The *pbp1* gene encodes a protein containing the

773 transmembrane helix (TM), N-terminal domain (N), transpeptidase (TP) domain and two

774 PASTA domains (P1 and P2). In the mutants, an ectopic copy of *pbp1* is placed under the

775 control of the P*spac* promoter at the lipase (*geh*) locus, whereas the gene in the native *pbp1*

776 locus is either deleted (Δ*pbp1*), has P1 and P2 domains removed (*pbp1*ΔPASTA), or has a point

777 mutation which results in inactivation of the TP domain (*pbp1**).

778 **b**, Schematic representation of domain architecture of PBP1 in *S. aureus* WT (*wt*) and PBP1

779 forms produced by Δ*pbp1*, *pbp1*ΔPASTA and *pbp1** mutants in the absence of inducer. The TP

780 domain inactivation is shown by dotted shading.

781 **c**, Immunoblot showing PBP1 levels in SH1000 *lacI* (*wt*) and in Δ*pbp1*, *pbp1*ΔPASTA and

782 *pbp1** grown with IPTG (+IPTG) and for 0, 1, 2 and 3 h without inducer (-IPTG) analysed

783 using anti-PBP1 antibody. Expected sizes: PBP1 and PBP1* = 83 kDa (black and grey

784 arrowheads, respectively) and PBP1ΔPASTA = 67 kDa (light blue arrowhead).

33

785 **d**, Plating efficiency of Δ*pbp1*, *pbp1*$_{ΔPASTA}$ and *pbp1** (MSSA) cells and MRSA *pbp1**

786 (*pbp1**$_{MRSA}$) cells upon inducer removal compared to the control groups grow in the presence

787 of inducer. *P* value was determined by Mann–Whitney *U* tests. $P = 0.0043$ (**, $P < 0.01$).

788 Data represent mean ± SD.

789 **e**, Growth curves of *pbp1** (MSSA) and MRSA *pbp1**(*pbp1**$_{MRSA}$) in the presence (+) or

790 absence (-) of IPTG. Data represent mean ± SD. Error bars that are smaller than the symbols

791 are not shown.

792

793 Data are representative of three (c, e) and at least four (d) independent experiments.

34

794
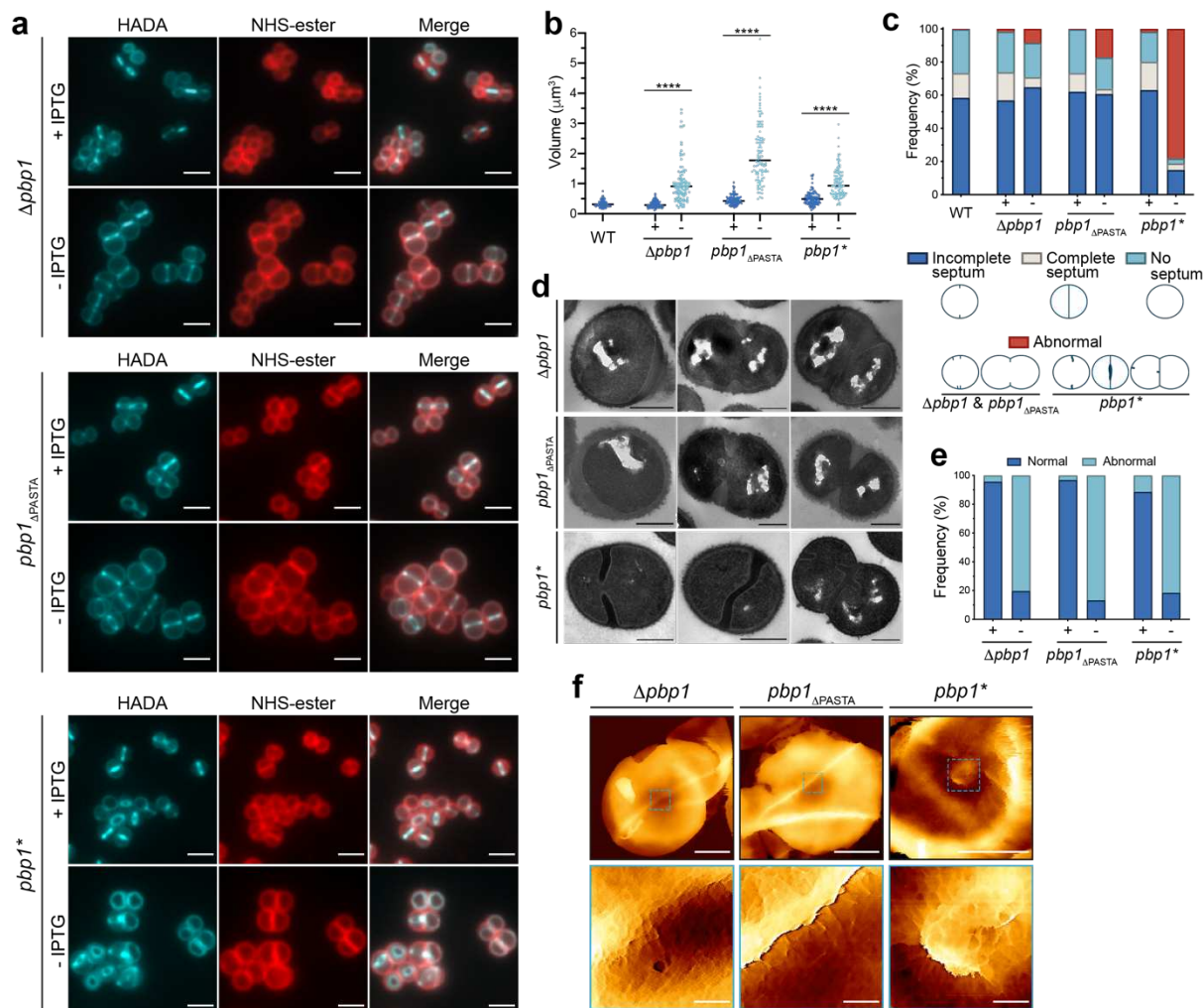
Fig. 2 The role of PBP1 in cell division and PG synthesis in *S. aureus.*

a, $\Delta pbp1$, $pbp1_{\Delta PASTA}$ and $pbp1*$ grown with or without IPTG for 2 h, incubated with HADA for 5 min to show nascent PG, and counter-labelled with NHS-ester Alexa Fluor 555 to image the cell wall. Images are average intensity projections of *z* stacks. Scale bars 2 μm.

b, Cell volumes of WT (*wt*), $\Delta pbp1$, $pbp1_{\Delta PASTA}$ and $pbp1*$ grown with (+) or without (-) IPTG for 2 h as measured by fluorescence microscopy after NHS-ester Alexa Fluor 555 labelling. Each dot represents a single cell. The median of each distribution is indicated by a black line. The number of cells analysed for each mutant and condition was $n \geq 100$. *P* value was determined by Mann–Whitney *U* tests (****, $P < 0.0001$). From left to right: $P = 3.033\text{e-}033$, $4.670\text{e-}049$ and $2.206\text{e-}022$; $n = 100, 101, 100, 101, 100, 100$ and 101.

35

805 **c**, Quantification of cellular phenotypes for WT *(wt)*, Δ*pbp1*, *pbp1*$_{\Delta PASTA}$ and *pbp1** based on

806 HADA incorporation (Fig. 2a) after incubation with (+) or without (-) IPTG for 2 h. From left

807 to right *n* = 370, 427, 332, 314, 364, 512 and 331.

808 **d**, TEM of Δ*pbp1*, *pbp1*$_{\Delta PASTA}$ and *pbp1** grown for 2 h in the absence of inducer. Scale bars

809 500 nm.

810 **e**, Quantification of cellular phenotypes based on TEM data of Δ*pbp1*, *pbp1*$_{\Delta PASTA}$ and *pbp1**

811 grown for 2 h in the presence (+) or absence (-) of IPTG. Examples of cells classified as

812 normal (blue) are shown in Fig. 2 – figure supplement 2b. Cells with abnormal phenotypes

813 (light blue) are shown in Fig. 2d and Fig. 2 – figure supplement 2c. From left to right *n* =

814 391, 329, 314, 377, 263 and 302.

815 **f**, AFM topographic images of internal surface of purified sacculi from Δ*pbp1*, *pbp1*$_{\Delta PASTA}$

816 and *pbp1** grown in the absence of inducer for 2 h. Sacculi (top images, scale bars 500 nm,

817 data scales (*z*): 450, 300 and 100 nm from left to right, respectively) and higher magnification

818 images (bottom images, scale bars 50 nm, data scales (*z*): 70, 100 and 50 nm from left to right

819 respectively) scanned within the boxed areas from the top images.

820

821 Data are representative of two (d-f) and (a-c) three independent experiments.

36
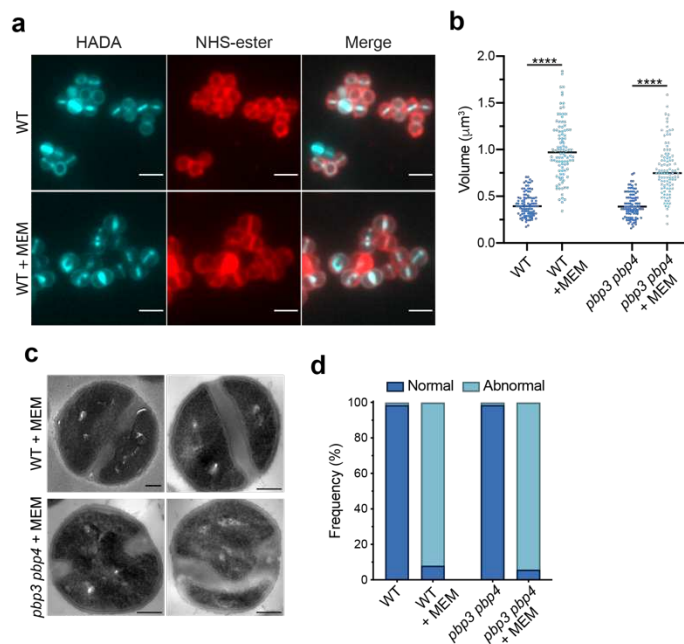
Fig. 3 Effect of meropenem (MEM), an antibiotic with high affinity for PBP1, on *S. aureus.*

a, Fluorescence images of SH1000 WT treated with 1x MIC MEM for 1 h, labelled with HADA for 5 min to show nascent PG and counter labelled with NHS-ester Alexa Fluor 555 (cell wall). Images are average intensity projections of *z* stacks. Scale bars 2 μm.

b, Cell volumes of SH1000 WT and *pbp3 pbp4* treated with 1x MIC MEM for 1 h as measured by fluorescence microscopy after NHS-ester Alexa Fluor 555 labelling (Fig. 3a). Each dot represents a single cell. The median of each distribution is indicated by a black line. The number of cells analysed for each condition was $n \geq 100$. *P* value was determined by Mann–Whitney *U* tests (****, $P < 0.0001$). From left to right: $P = 1.276\text{e-}042$ and $1.421\text{e-}024$; $n = 102, 100, 101$ and 102.

**c**, TEM of SH1000 WT and *pbp3 pbp4* treated with 1x MIC MEM for 1 h. Scale bars 200 nm.

d, Quantification of phenotypes of SH1000 WT and *pbp3 pbp4* treated with MEM (1x MIC) for 1 h based on TEM data (Fig. 3c and Fig. 3 – figure supplement 1e, f). Examples of cells classified as normal (blue) are shown in Fig. 3 – figure supplement 1e, f. Cells with abnormal

839   phenotypes (light blue) are shown in Fig. 3c and Fig. 3 – figure supplement 1e, f. From left to

840   right *n*= 343, 287, 275 and 172.

841

842   Data are representative of two (a, b (for WT) independent experiments. Experiments in b (for

843   *pbp3 pbp4)* and d were performed once.

844

845
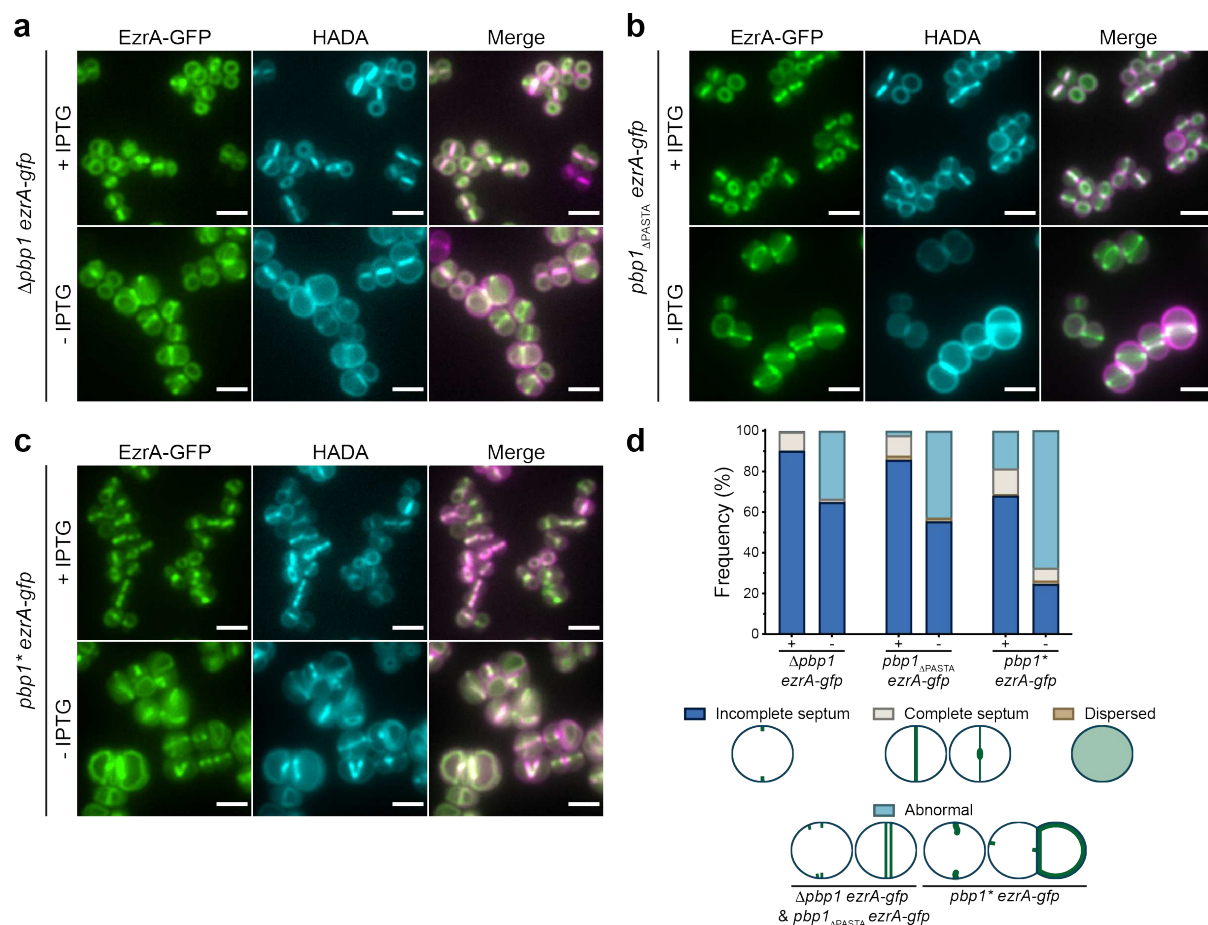
Fig. 4 The role of PBP1, PASTA and TP domains in EzrA localisation in *S. aureus.*

a-c, Localisation of EzrA-GFP in Δ*pbp1 ezrA-gfp, pbp1*ΔPASTA *ezrA-gfp* and *pbp1* ezrA-gfp*

grown in the presence or absence of IPTG for 2 h and labelled with HADA for 5 min to stain

PG. Images are average intensity projections of *z* stacks. Scale bars 5 μm.

d, Quantification of EzrA-GFP localisations in Δ*pbp1 ezrA-gfp, pbp1*ΔPASTA *ezrA-gfp* and

pbp1* ezrA-gfp grown with or without IPTG. From left to right *n* = 395, 499, 481, 438, 360

and 382.

Data are representative of two independent experiments.
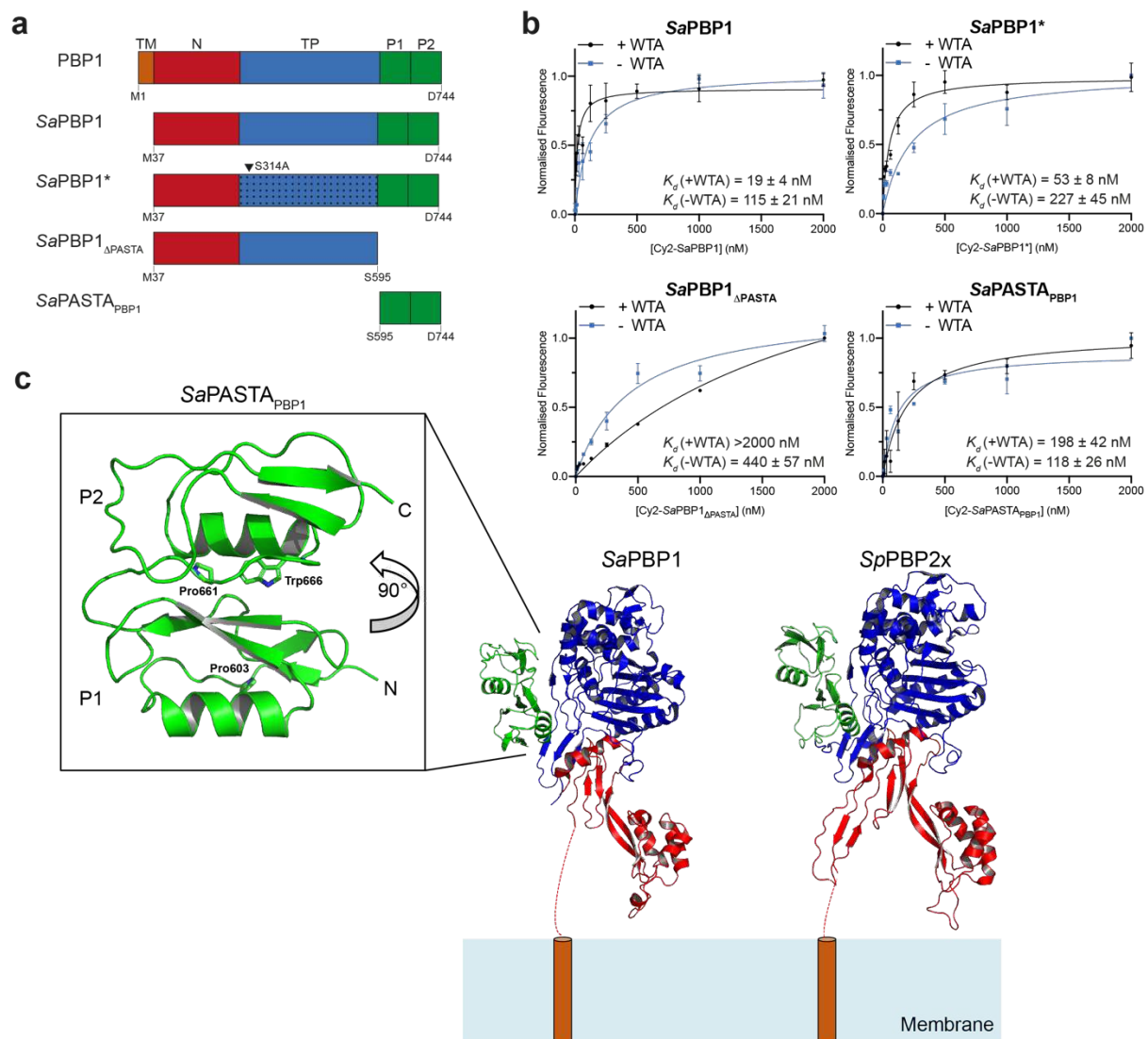
Fig. 5 Role of PBP1 PASTA domains in cell wall binding

a, Schematic representation of structural domain organization of *S. aureus* PBP1 (top) and recombinant proteins (*Sa*PBP1, *Sa*PBP1$_{\Delta PASTA}$, *Sa*PBP1* and *Sa*PASTA$_{PBP1}$) used in this study. TM, trans-membrane helix (orange); N, N-terminal dimerization domain (red); TP, transpeptidase domain (blue); P, PASTA domains (green). The arrowhead indicates the inactivation substitution in the TP domain of *Sa*PBP1*. The first and last amino acids of constructs are indicated.

b, Fluorescent cell wall sedimentation assay. A Wilcoxon signed rank test ($P < 0.05$) was carried out to assess the significance of difference in +WTA/-WTA PG binding: *Sa*PBP1, $P = 0.0273$; *Sa*PBP1*, $P = 0.0078$; *Sa*PBP1$_{\Delta PASTA}$, $P = 0.0195$; *Sa*PASTA$_{PBP1}$, $P \geq 0.9999$,

866   not significant. Data represent mean $\pm$ SD. Error bars that are smaller than the symbols are

867   not shown.

868   **c**, Structure of SaPASTA$_{PBP1}$. The crystal structure of *S. aureus* PBP1 lacking the PASTA

869   domains (SaPBP1, PDB 5TRO) and our SaPASTA$_{PBP1}$ structure were superimposed on to *S.*

870   *pneumoniae* PBP2x (SpPBP2x, PDB 5OAU) and displayed as cartoons. Their N-termini are

871   orientated close to the representative cell membrane, as if anchored there by their respective

872   transmembrane helices (dashed red line/orange cylinder). Individual domains are coloured as
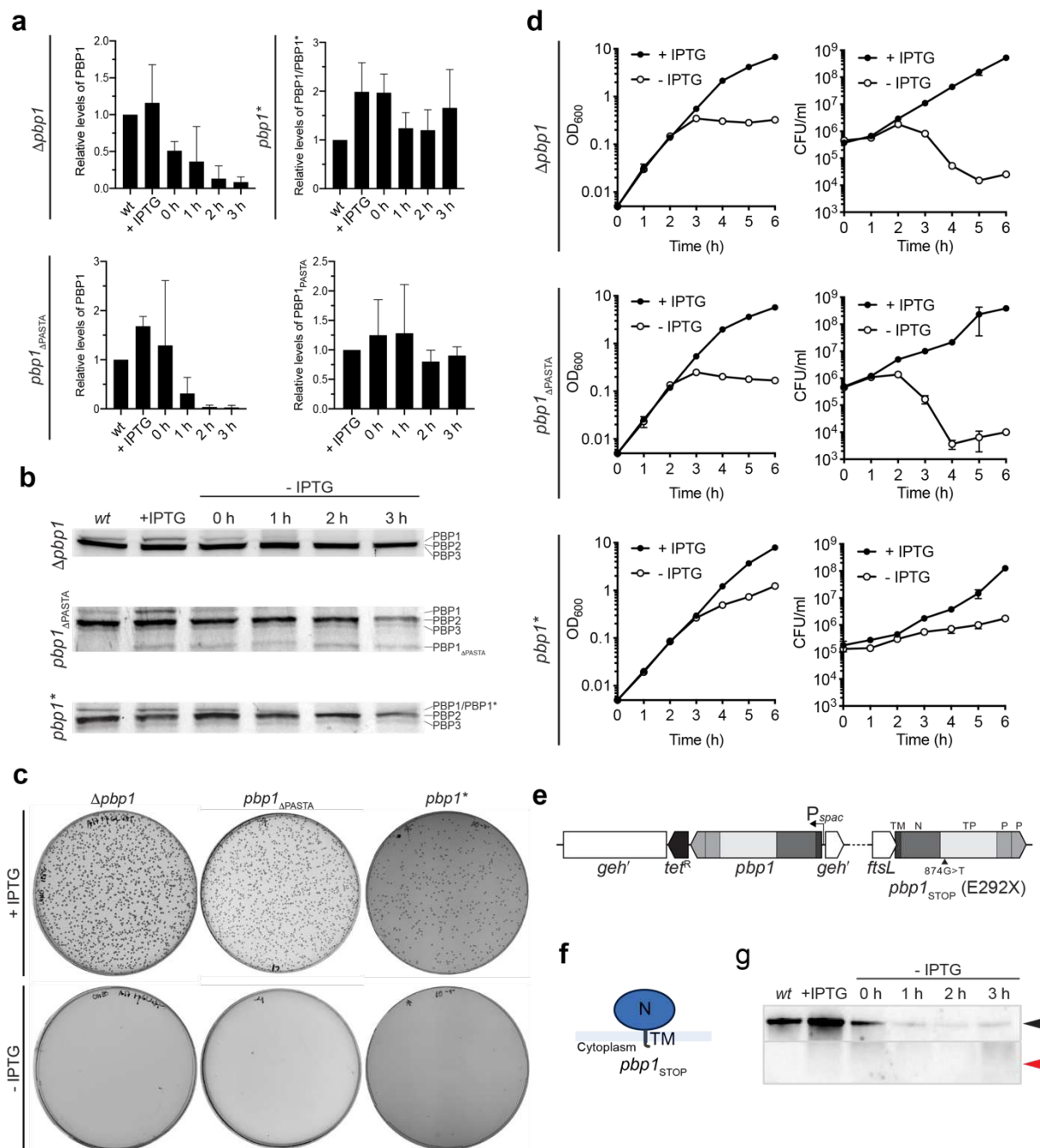
873   follows; N-terminal domain (red), transpeptidase domain (blue) and PASTA domain (green).

874   The individual PASTA domains are labelled P1 and P2, respectively. Residues Pro603,

875   Pro661 and Trp666 are displayed as sticks, with nitrogen atoms coloured blue.

Supplementary figures and legends
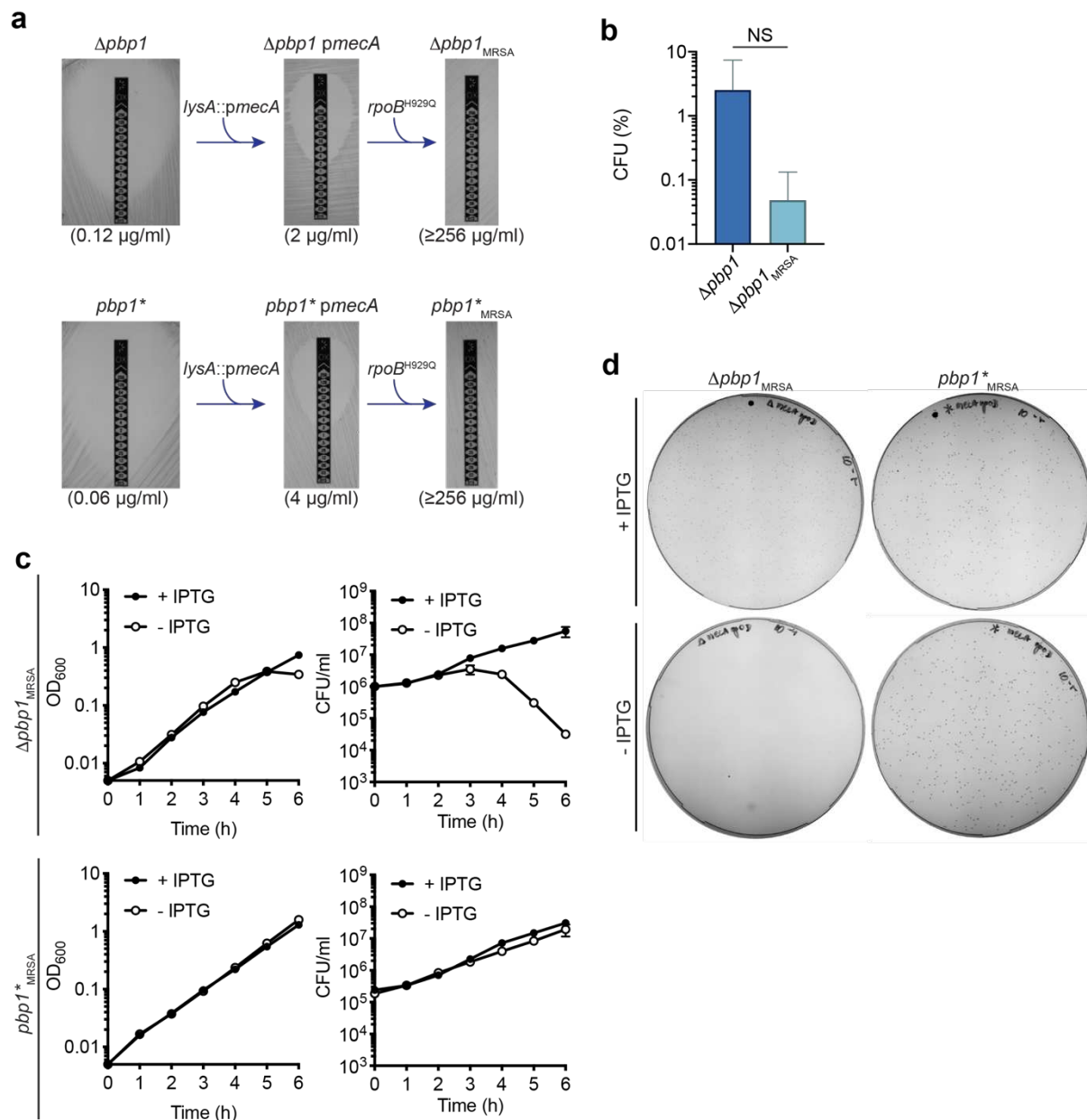

Fig. 1 – figure supplement 1. Essentiality of PBP1, PASTA and TP domains in *S. aureus*.

a, Relative levels of PBP1 in Δ*pbp1, pbp1*$_{\Delta PASTA}$ and *pbp1** grown with IPTG and for 0, 1, 2 and 3 h after inducer removal. PBP1 levels were normalized to protein levels in SH1000 *lacI*

42

882   (*wt*). PBP1$_{\Delta PASTA}$ levels were normalized to PBP1$_{\Delta PASTA}$ levels in the presence of inducer.

883   Quantifications are for the data shown in Fig. 1c. Data represent mean ± SD.

884   **b**, BocillinFL gel-based analysis of penicillin binding proteins in SH1000 *lacI* (*wt*) and

885   Δ*pbp1, pbp1*$_{\Delta PASTA}$ and *pbp1** grown with IPTG and 0, 1, 2 and 3 h after inducer removal.

886   **c**, Growth of Δ*pbp1, pbp1*$_{\Delta PASTA}$ and *pbp1** with or without IPTG. Quantifications for the

887   plate assay are shown in Fig. 1d.

888   **d**, Growth curves of Δ*pbp1, pbp1*$_{\Delta PASTA}$ and *pbp1** in the presence or absence of IPTG. Data

889   represent mean ± SD. Error bars that are smaller than the data point symbols are not shown.

890   **e**, Schematic representation of the *pbp1*$_{STOP}$ mutant. A SNP (874 G for T) resulted in a

891   premature stop codon (E292X) and removal of the TP and PASTA domains.

892   **f**, Schematic representation of domain architecture of PBP1$_{STOP}$ encoded by the *pbp1*$_{STOP}$

893   mutant.

894   **g**, Immunoblot showing PBP1 levels in SH1000 *lacI* (*wt*) and *pbp1*$_{STOP}$ grown with IPTG and

895   for 0, 1, 2 and 3 h without inducer analysed using anti-PBP1 antibody. Expected sizes: PBP1

896   = 83 kDa (black arrowhead) and PBP1$_{STOP}$ = 33 kDa (red arrowhead).

897

898   Data are representative of two (g), three (a, b, d) and at least four (c) independent

899   experiments.

Fig. 1 – figure supplement 2. Essentiality of PBP1 and its TP activity in Methicillin-resistant *S. aureus*.

a, Schematic representation of evolution of high-level β-lactam resistant Δ*pbp1* and *pbp1**. A single copy *mecA* under its native promoter (p*mecA*) was introduced at the *lysA* locus, resulting in low-level oxacillin resistant Δ*pbp1* p*mecA* and *pbp1** p*mecA*. Subsequently, addition of a point mutation in the *rpoB* gene results in development of high-level resistant Δ*pbp1*MRSA and *pbp1**. Oxacillin MICs shown in brackets were measured using the E-test strips.

44

909   **b**, Plating efficiency of Δ*pbp* (MSSA) and MRSA Δ*pbp1*$_{MRSA}$ cells upon the inducer removal

910   compared to the control groups grown in the presence of inducer. Data represent mean ± SD.

911   *P* value was determined by Mann–Whitney *U* tests. *P* = 0.5429 (NS, not significant).

912   **c**, Growth curves of Δ*pbp1*$_{MRSA}$ and *pbp1**$_{MRSA}$ in the presence or absence of IPTG. Data

913   represent mean ± SD. Error bars that are smaller than the data point symbols are not shown.

914   **d**, Growth of Δ*pbp1*$_{MRSA}$ and *pbp1**$_{MRSA}$ with or without IPTG. Quantifications for

915   Δ*pbp1*$_{MRSA}$ are shown in Fig. 1 – figure supplement 2c and for *pbp1**$_{MRSA}$ are shown in Fig.

916   1b.

917

918   Data are representative of at least three independent experiments.
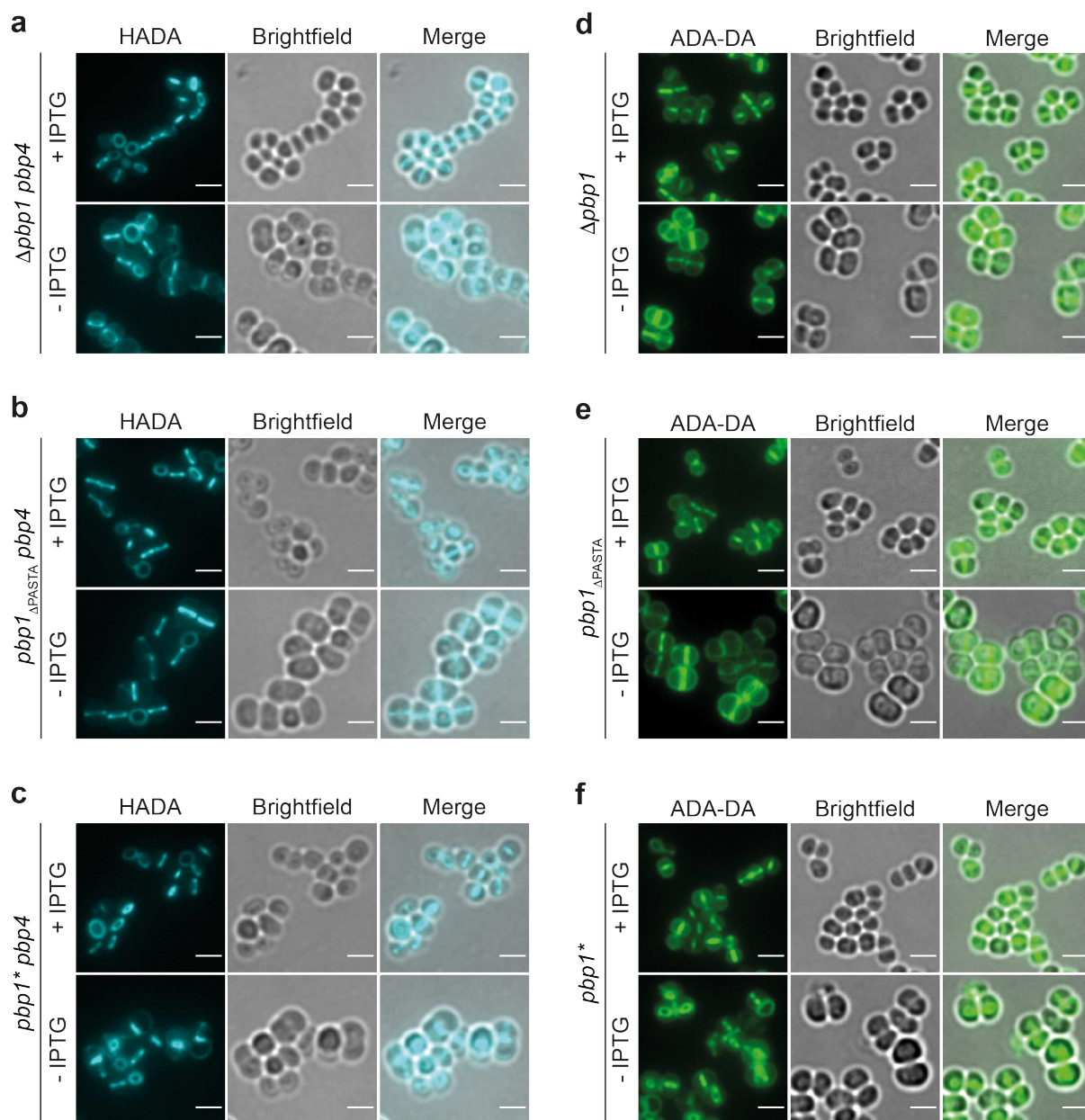
Fig. 2 – figure supplement 1. Loss of PBP1, PASTAs or TP activity of PBP1 does not prevent PG synthesis.

a-c, PG incorporation in *pbp4* mutants depleted of PBP1. Δ*pbp1 pbp4, pbp1*$_{\Delta PASTA}$ *pbp4* and *pbp1* pbp4* grown with or without IPTG for 2 h and incubated with HADA for 5 min to show nascent PG incorporation.

d-f, Δ*pbp1, pbp1*$_{\Delta PASTA}$ and *pbp1** grown with or without IPTG for 2 h, incubated with dipeptide (ADA-DA) for 5 min and clicked to Alexa Fluor 488 to show nascent PG incorporation.

46

928   Fluorescence images are average intensity projections of *z* stacks. Scale bars 2 μm.

929   47

930   Images are representatives of two independent experiments.

931
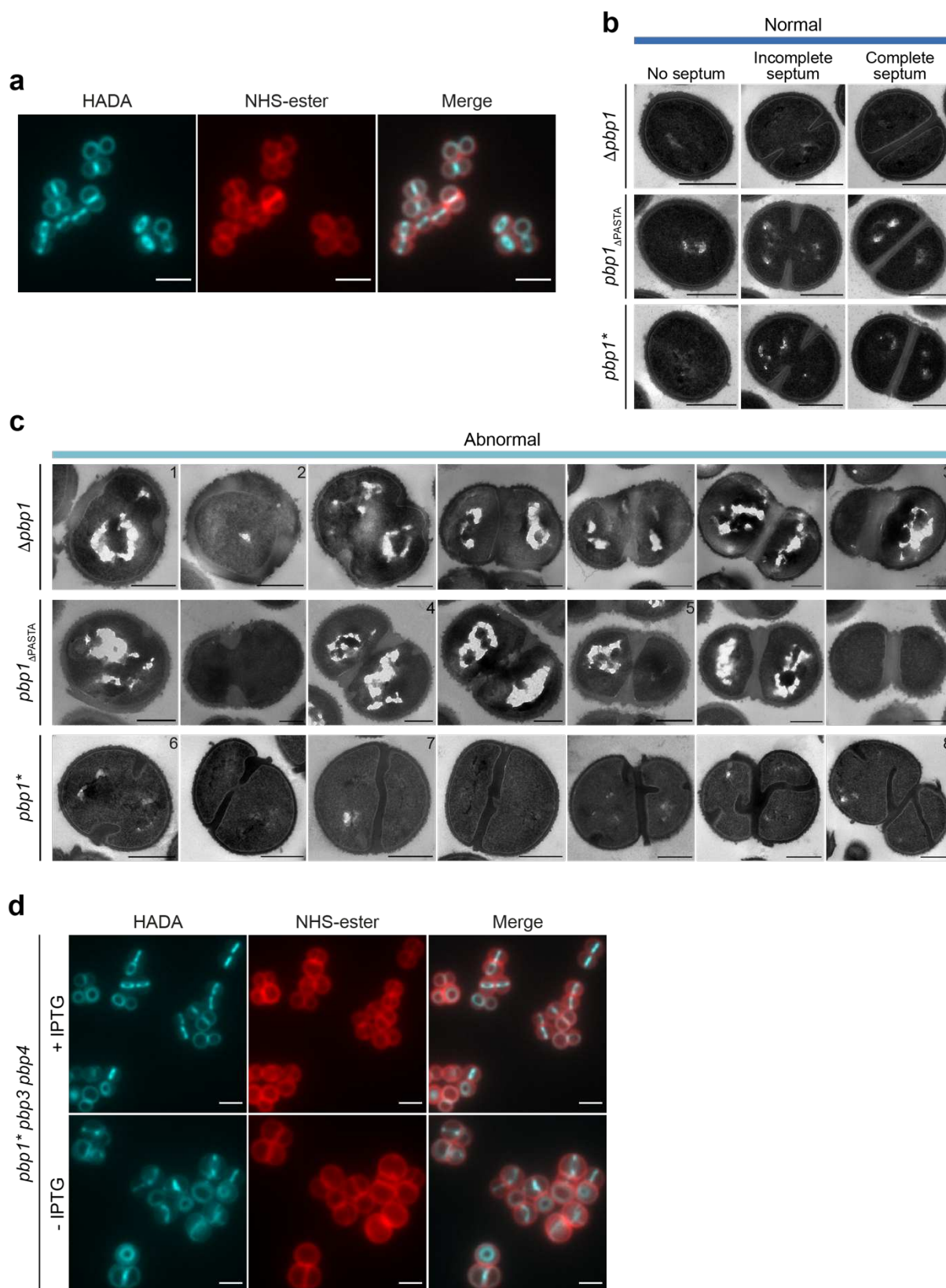
Fig. 2 – figure supplement 2. Role of PBP1 in *S. aureus*

933 **a**, Fluorescence images of SH1000 WT labelled with HADA for 5 min (nascent PG) and

934 counter labelled with NHS-ester Alexa Fluor 555 (cell wall). Images are average intensity

935 projections of z stacks. Scale bars 2 μm.

936 **b**, TEM of Δ*pbp1*, *pbp1*$_{\Delta PASTA}$ and *pbp1** grown in the presence of IPTG categorised as

937 normal phenotype (blue). Scale bars 500 nm.

938 **c**, TEM of Δ*pbp1*, *pbp1*$_{\Delta PASTA}$ and *pbp1** grown in the absence of IPTG for 2 h categorised

939 as abnormal phenotype (1, PG blebs; 2, thickened cell wall; 3, thickened complete septum; 4,

940 multiple septa; 5, misshapen incomplete septum; 6, thick incomplete septum with rounded

941 leading edge; 7, curved septum; 8, separation defect. Scale bars 500 nm.

942 **d**, Fluorescence images of *pbp1* pbp3 pbp4* grown with or without IPTG for 2 h, labelled

943 with HADA for 5 min (nascent PG) and counter stained with NHS-ester Alexa Fluor 555

944 (cell wall). Images are average intensity projections of z stacks. Scale bars 2 μm.

945

946 Data are representative of two independent experiments.
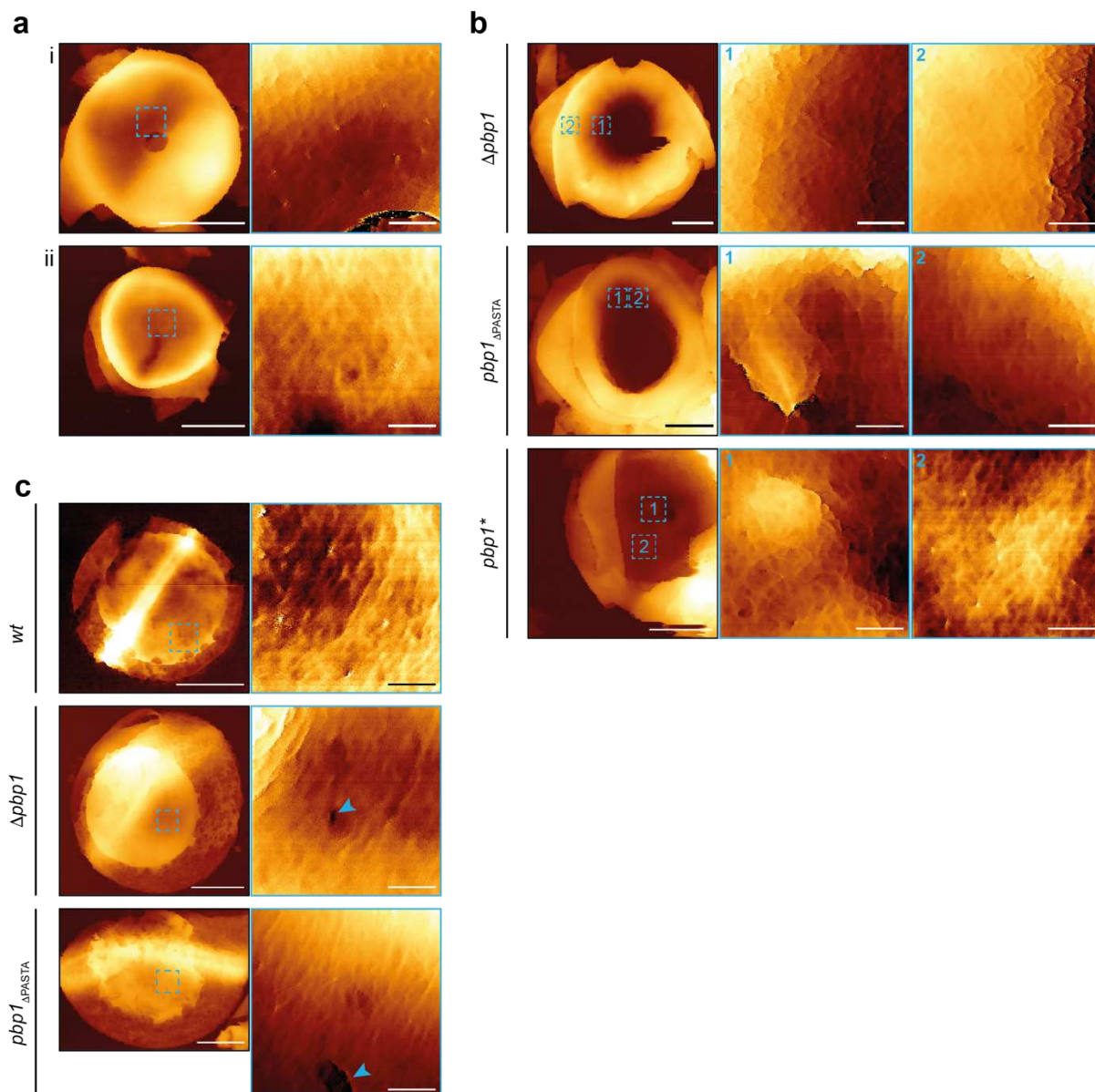
Fig. 2 – figure supplement 3. Gallery of AFM images of *S. aureus* Δ*pbp1, pbp1*ΔPASTA and *pbp1*

a, AFM topographic images of unfinished (i) and closed (ii) septa in *S. aureus* SH1000. Sacculi (images to the left, scale bars 500 nm, data scales (*z*): 200 (top) and 250 nm (bottom)) and higher magnification scans (images to the right, scale bars 50 nm, data scales (*z*): 80 (top) and 40 nm (bottom)) on the boxed areas from the images to the left.

b, AFM topographic images of unfinished septa in Δ*pbp1* (from left to right: scale bars 500, 50 and 50 nm; data scales (*z*) 500, 120 and 150 nm), *pbp1*ΔPASTA (from left to right: scale bars 500, 50 and 50 nm; data scales (*z*) 693, 80 and 100 nm) and *pbp1** (from left to right: scale

957   bars 500, 50 and 50 nm; data scales (z) 500, 80 and 25 nm) grown in the absence of inducer

958   for 2 h. Images to the left are sacculi, while images in the centre (1) and to the right (2) are

959   higher magnification scans on the boxed areas of the images on the left.

960   **c**, AFM topographic images of external nascent ring architecture in SH1000 WT (*wt*; scale

961   bars: from left to right: scale bars 500 and 50 nm; data scales (z) 100 and 20 nm) and mutants

962   Δ*pbp1* (scale bars: from left to right: scale bars 500 and 50 nm; data scales (z) 400 and 60

963   nm) and *pbp1*$_{\Delta PASTA}$ (scale bars: from left to right: scale bars 500 and 50 nm; data scales (z)

964   350 and 100 nm) grown in the absence of inducer for 2 h. Images to the left are sacculi, while

965   images to the right are higher magnification scans on the boxed areas of the images on the

966   left. The arrowheads indicate abnormal features, holes.

967

968   Data are representative of two independent experiments.
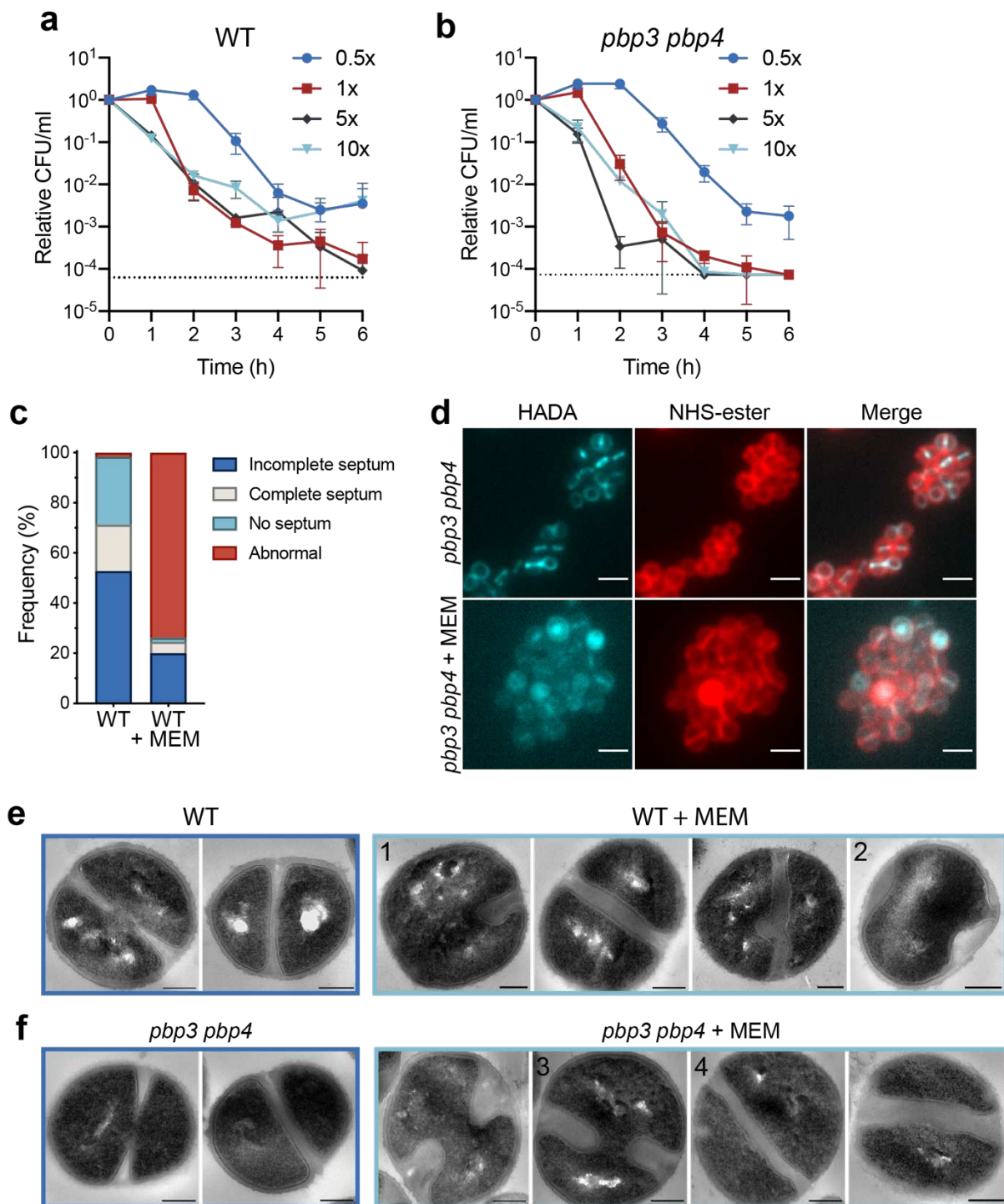
Fig. 3 – figure supplement 1. Effect of meropenem (MEM) on *S. aureus.*

a-b, Bactericidal effect of addition of 0.5x, 1x, 5x and 10x MIC MEM on (a) SH1000 WT and (b) *pbp3 pbp4* (b). MEM MIC is 0.4 µg/ml and 0.2 µg/ml for SH1000 WT and *pbp3 pbp4*, respectively Data represent mean ± SD. Error bars that are symbols than the dots are not shown. The dotted line is the detection limit.

975 **c**, Quantification of cellular phenotypes of SH1000 WT treated with 1x MIC MEM for 1 h

976 based on HADA incorporation (Fig 3a). Same phenotype classification was used as shown in

977 Fig. 2c. From left to right n = 309 and 355.

978 **d**, Fluorescence images of *pbp3 pbp4* treated with 1x MIC MEM for 1 h, labelled with

979 HADA for 5 min to show nascent PG and counter labelled with NHS-ester Alexa Fluor 555

980 (cell wall). Images are average intensity projections of z stacks. Scale bars 2 μm. Phenotype

981 classification of MEM treated *pbp3 pbp4* was not possible due to low HADA fluorescence

982 signal.

983 **e-f,** TEM of SH1000 WT (e) and *pbp3 pbp4* (f) grown with or without 1x MIC MEM for 1 h.

984 Scale bars 200 nm. Examples of cells categorised as normal phenotype are in blue, cells with

985 abnormal phenotype are in light blue (1, asymmetric septum ingrowth; 2, off-septal PG

986 thickening; 3, septum with rounded leading edge; 4, curved septum).

987

988 Data are representative of three (a and b) and two (c) independent experiments. Experiments

989 in d, e and f were performed once.

990
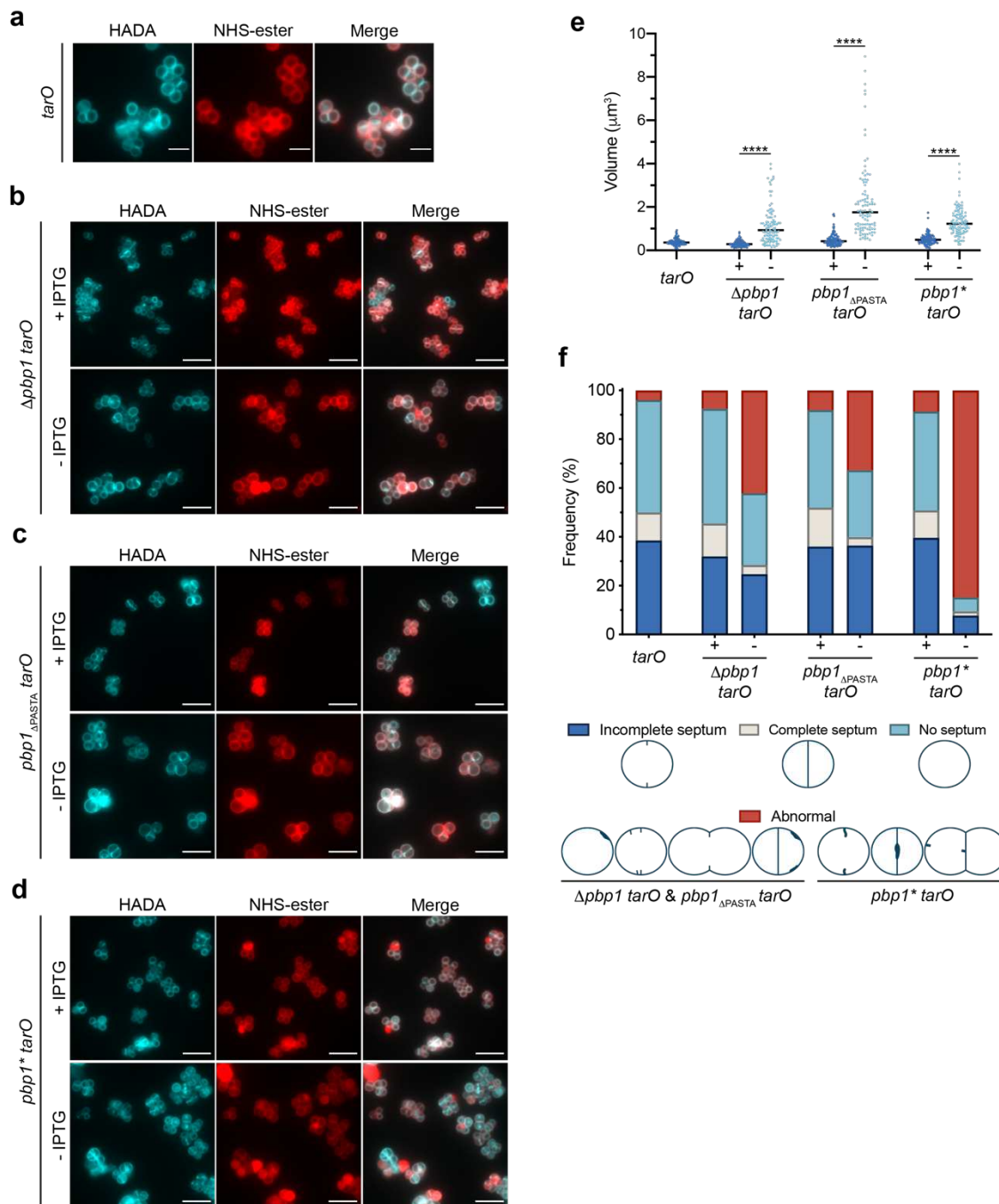
Fig. 4 – figure supplement 1. Functional association between PBP1 and WTA

a, Fluorescence images of the *tarO* mutant labelled with HADA for 5 min (nascent PG) and counter stained with NHS-ester Alexa Fluor 555 (cell wall). Images are average intensity projections of *z* stacks. Scale bars 5 μm.

b-d, Δ*pbp1 tarO, pbp1*ₐₚₐₛₜₐ *tarO* and *pbp1* tarO* grown with or without IPTG for 2 h, incubated with HADA for 5 min to show nascent PG and counter labelled with NHS-ester

54

997　　Alexa Fluor 555 (cell wall). Images are average intensity projections of *z* stacks. Scale bars 5

998　　μm.

999　　**e**, Cell volumes of *tarO* and Δ*pbp1 tarO, pbp1*$_{ΔPASTA}$ *tarO* and *pbp1* tarO* grown with or

1000　　without IPTG as measured by fluorescence microscopy after NHS-ester Alexa Fluor 555

1001　　labelling. Each dot represents a single cell. The median of each distribution is indicated by a

1002　　black line. The number of cells analysed for each mutant and condition was $n \geq 100$. *P* value

1003　　was determined by Mann–Whitney *U* tests (***, $P < 0.0001$). From left to right: $P = 2.243e\text{-}$

1004　　022, $1.460e\text{-}037$ and $8.074e\text{-}029$; $n = 100, 102, 101, 100, 100, 100$ and 100.

1005　　**f**, Quantification of cellular phenotypes for *tarO* and Δ*pbp1 tarO, pbp1*$_{ΔPASTA}$ *tarO* and

1006　　*pbp1* tarO* based on HADA incorporation (Fig. 4 – figure supplement 1a-d) after incubation

1007　　with or without IPTG. From left to right $n = 306, 253, 271, 358, 266, 313$ and 336.

1008

1009　　Data are representative of two independent experiments.

55
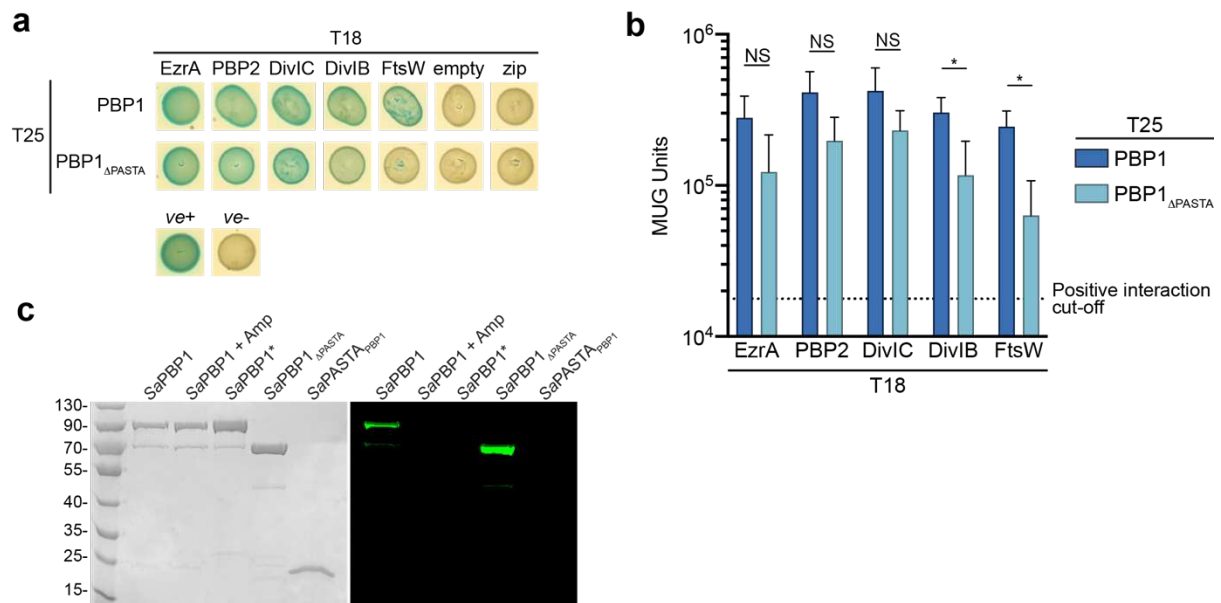
1010

1011 **Fig. 5 – figure supplement 1. The role of PBP1 PASTA domains in interactions with cell**

1012 **division components and PG.**

1013 **a**, Bacterial two-hybrid analysis of the effect of PASTA domains truncation on PBP1

1014 interaction with its known interaction partners; empty, T18 with no insert; zip, T18 with a

1015 leucine zipper fragment; *ve+*, positive control (T18-zip/T25-zip); *ve-*, negative control

1016 (T18/T25).

1017 **b**, Quantitative bacterial two-hybrid analysis of the effect of the PASTA domains truncation

1018 on PBP1 interaction with cell division components determined by analysis of the β-

1019 galactosidase activities of *E. coli* BTH101 cells harbouring the corresponding plasmids.

1020 Dotted line, the positive interaction cut off value (4-fold greater than the pair of T18/T25).

1021 Data represent mean ± SD. *P* value was determined by Mann–Whitney *U* tests (*, $P < 0.05$).

1022 DivIB (PBP1 *vs* PBP1$_{\Delta PASTA}$) $P = 0.0424$, FtsW (PBP1 *vs* PBP1$_{\Delta PASTA}$) $P = 0.0163$.

1023 **c**, Coomassie-stained SDS-PAGE gel (left) and BocillinFL gel-based analysis (right) of

1024 purified recombinant *Sa*PBP1, *Sa*BPP1*, *Sa*PBP1$_{\Delta PASTA}$ and *Sa*PASTA$_{PBP1}$. Bands

1025 corresponding to *Sa*PBP1 and *Sa*PBP1$_{\Delta PASTA}$ were fluorescent, indicating their covalent

1026 binding to BocillinFL. Bands corresponding to *Sa*PBP1* and *Sa*PASTA$_{PBP1}$ were not

1027 fluorescent, and were therefore unable to bind BocillinFL. *Sa*PBP1 incubated with ampicillin

56

1028   prior to BocillinFL incubation failed to fluoresce, consistent with specific binding of

1029   BocillinFL to the TP domain. Expected sizes: SaPBP1 and SaPBP1*, 80.5kDa;

1030 SaPBP1$_{\Delta PASTA}$, 64.5 kDa; SaPASTA$_{PBP1}$, 18.2 kDa.

1031

1032   Data are representative of two (c) and three (a-b) independent experiments.
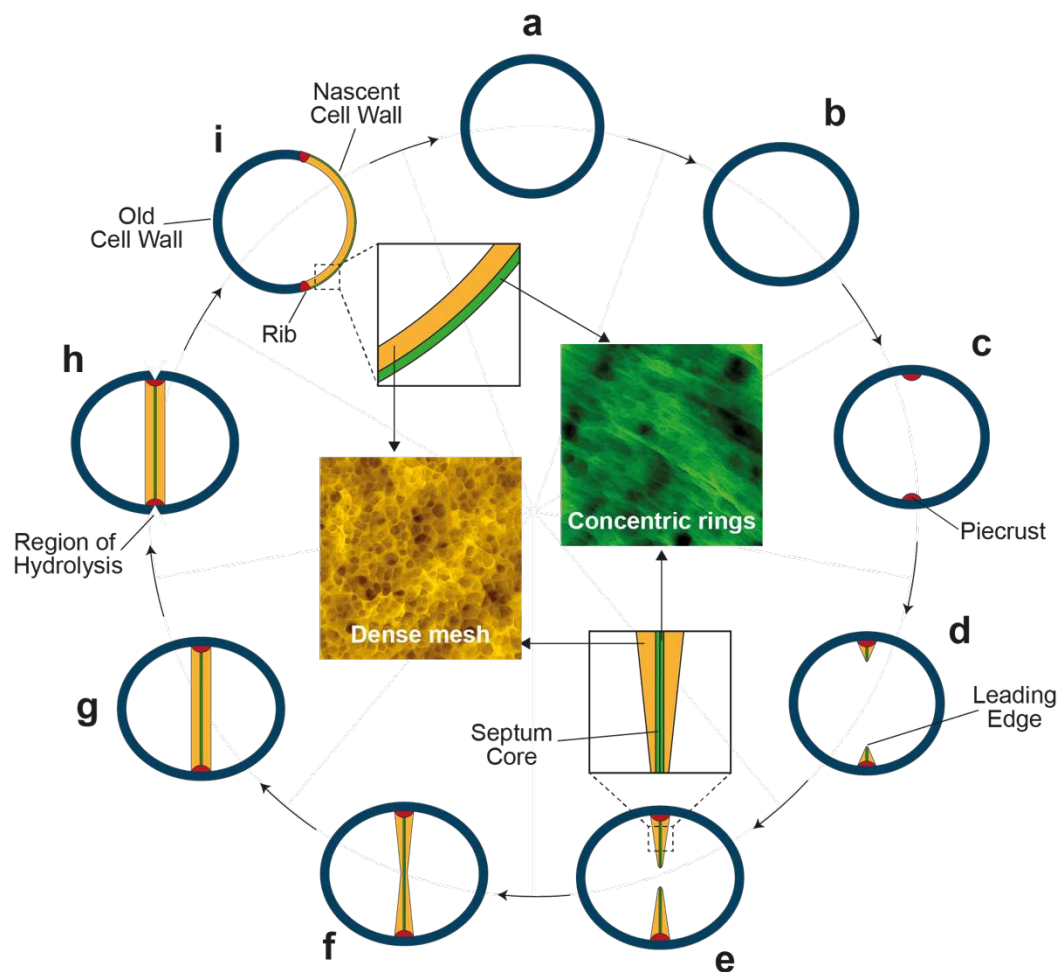
1033

Fig. 5 – figure supplement 2. Conceptual model of septum formation in *S. aureus*.

(a, b) The growing *S. aureus* cell increases in volume (Zhou et al., 2015). (c) Septal synthesis starts by formation of the piecrust (red) (Turner et al., 2010). (d. e) 'V' shaped septum (Lund et al., 2018) progresses inwards by insertion of ring like structured PG synthesised by PBP1-FtsW at the septum core and mesh structured PG produced by PBP2. (f) The annulus closes resulting in a bowed septum. (g) Septum is filled out by peptidoglycan insertion executed by PBP2 and this continues until the cross wall is of uniform thickness (Lund et al., 2018). (h) Cell wall is hydrolysed at the plane of septation. (i) Daughter cells separate. The cell wall of the daughter cell (coloured insets) is a chimera of the old cell wall with both internally and externally mesh structured PG and a nascent cell wall with the external ring structured PG and the mesh-like cytoplasmic facing PG (Pasquina-Lemonche et al., 2020).

58

References

Arnaud, M., Chastanet, A., & Débarbouillé, M. (2004). New vector for efficient allelic replacement in naturally nontransformable, low-GC-content, gram-positive bacteria. *Applied and Environmental Microbiology*, *70*(11), 6887–6891. https://doi.org/10.1128/AEM.70.11.6887-6891.2004

Atilano, M. L., Pereira, P. M., Yates, J., Reed, P., Veiga, H., Pinho, M. G., & Filipe, S. R. (2010). Teichoic acids are temporal and spatial regulators of peptidoglycan cross-linking in Staphylococcus aureus. *Proceedings of the National Academy of Sciences of the United States of America*, *107*(44), 18991–18996. https://doi.org/10.1073/pnas.1004304107

Barthe, P., Mukamolova, G. V., Roumestand, C., & Cohen-Gonsaud, M. (2010). The Structure of PknB Extracellular PASTA Domain from Mycobacterium tuberculosis Suggests a Ligand-Dependent Kinase Activation. *Structure*, *18*(5), 606–615. https://doi.org/10.1016/j.str.2010.02.013

Bernardo-García, N., Mahasenan, K. V., Batuecas, M. T., Lee, M., Hesek, D., Petráčková, D., Doubravová, L., Branny, P., Mobashery, S., & Hermoso, J. A. (2018). Allostery, Recognition of Nascent Peptidoglycan, and Cross-linking of the Cell Wall by the Essential Penicillin-Binding Protein 2x of Streptococcus pneumoniae. *ACS Chemical Biology*, *13*(3), 694–702. https://doi.org/10.1021/acschembio.7b00817

Berrow, N. S., Alderton, D., & Owens, R. J. (2009). The precise engineering of expression vectors using high-throughput In-Fusion PCR cloning. *Methods in Molecular Biology (Clifton, N.J.)*, *498*, 75–90. https://doi.org/10.1007/978-1-59745-196-3_5

Berti, A. D., Sakoulas, G., Nizet, V., Tewhey, R., & Rose, W. E. (2013). β-Lactam Antibiotics Targeting PBP1 Selectively Enhance Daptomycin Activity against

1069   Methicillin-Resistant Staphylococcus aureus. *Antimicrobial Agents and*

1070   *Chemotherapy*, *57*(10), 5005–5012. https://doi.org/10.1128/AAC.00594-13

1071   Bertsche, U., Kast, T., Wolf, B., Fraipont, C., Aarsman, M. E. G., Kannenberg, K., von

1072   Rechenberg, M., Nguyen-Distèche, M., den Blaauwen, T., Höltje, J.-V., & Vollmer,

1073   W. (2006). Interaction between two murein (peptidoglycan) synthases, PBP3 and

1074   PBP1B, in Escherichia coli. *Molecular Microbiology*, *61*(3), 675–690.

1075   https://doi.org/10.1111/j.1365-2958.2006.05280.x

1076   Bottomley, A. L., Kabli, A. F., Hurd, A. F., Turner, R. D., Garcia-Lara, J., & Foster, S. J.

1077   (2014). Staphylococcus aureus DivIB is a peptidoglycan-binding protein that is

1078   required for a morphological checkpoint in cell division. *Molecular Microbiology*.

1079   https://doi.org/10.1111/mmi.12813

1080   Bunkóczi, G., & Read, R. J. (2011). Improvement of molecular-replacement models with

1081   Sculptor. *Acta Crystallographica. Section D, Biological Crystallography*, *67*(Pt 4),

1082   303–312. https://doi.org/10.1107/S0907444910051218

1083   Calvanese, L., Falcigno, L., Squeglia, F., D'Auria, G., & Berisio, R. (2017). Structural and

1084   dynamic features of PASTA domains with different functional roles. *Journal of*

1085   *Biomolecular Structure and Dynamics*, *35*(10), 2293–2300.

1086   https://doi.org/10.1080/07391102.2016.1217274

1087   Campbell, J., Singh, A. K., Santa Maria, J. P., Kim, Y., Brown, S., Swoboda, J. G.,

1088   Mylonakis, E., Wilkinson, B. J., & Walker, S. (2011). Synthetic lethal compound

1089   combinations reveal a fundamental connection between wall teichoic acid and

1090   peptidoglycan biosyntheses in Staphylococcus aureus. *ACS Chemical Biology*, *6*(1),

1091   106–116. https://doi.org/10.1021/cb100269f

1092   Chen, V. B., Arendall, W. B., Headd, J. J., Keedy, D. A., Immormino, R. M., Kapral, G. J.,

1093   Murray, L. W., Richardson, J. S., & Richardson, D. C. (2010). MolProbity: All-atom

1094   structure validation for macromolecular crystallography. *Acta Crystallographica.*

1095   *Section D, Biological Crystallography*, *66*(Pt 1), 12–21.

1096   https://doi.org/10.1107/S0907444909042073

1097   Cho, H., Wivagg, C. N., Kapoor, M., Barry, Z., Rohs, P. D. A., Suh, H., Marto, J. A., Garner,

1098   E. C., & Bernhardt, T. G. (2016). Bacterial cell wall biogenesis is mediated by SEDS

1099   and PBP polymerase families functioning semi-autonomously. *Nature Microbiology*,

1100   *1*(10), 1–8. https://doi.org/10.1038/nmicrobiol.2016.172

1101   Cooper, E. L., García-Lara, J., & Foster, S. J. (2009). YsxC, an essential protein in

1102   Staphylococcus aureus crucial for ribosome assembly/stability. *BMC Microbiology*, *9*,

1103   266. https://doi.org/10.1186/1471-2180-9-266

1104   Emsley, P., Lohkamp, B., Scott, W. G., & Cowtan, K. (2010). Features and development of

1105   Coot. *Acta Crystallographica. Section D, Biological Crystallography*, *66*(Pt 4), 486–

1106   501. https://doi.org/10.1107/S0907444910007493

1107   Erster, O., & Liscovitch, M. (2010). A modified inverse PCR procedure for insertion,

1108   deletion, or replacement of a DNA fragment in a target sequence and its application in

1109   the ligand interaction scan method for generation of ligand-regulated proteins.

1110   *Methods in Molecular Biology (Clifton, N.J.)*, *634*, 157–174.

1111   https://doi.org/10.1007/978-1-60761-652-8_12

1112   Evans, P. R., & Murshudov, G. N. (2013). How good are my data and what is the resolution?

1113   *Acta Crystallographica. Section D, Biological Crystallography*, *69*(Pt 7), 1204–1214.

1114   https://doi.org/10.1107/S0907444913000061

1115   Farha, M. A., Leung, A., Sewell, E. W., D'Elia, M. A., Allison, S. E., Ejim, L., Pereira, P.

1116   M., Pinho, M. G., Wright, G. D., & Brown, E. D. (2013). Inhibition of WTA synthesis

1117   blocks the cooperative action of PBPs and sensitizes MRSA to β-lactams. *ACS*

1118   *Chemical Biology*, *8*(1), 226–233. https://doi.org/10.1021/cb300413m

1119 Fey, P. D., Endres, J. L., Yajjala, V. K., Widhelm, T. J., Boissy, R. J., Bose, J. L., & Bayles,

1120   K. W. (2013). A genetic resource for rapid and comprehensive phenotype screening

1121   of nonessential Staphylococcus aureus genes. *MBio*, *4*(1), e00537-00512.

1122   https://doi.org/10.1128/mBio.00537-12

1123 García-Lara, J., Weihs, F., Ma, X., Walker, L., Chaudhuri, R. R., Kasturiarachchi, J.,

1124   Crossley, H., Golestanian, R., & Foster, S. J. (2015). Supramolecular structure in the

1125   membrane of Staphylococcus aureus. *Proceedings of the National Academy of*

1126   *Sciences*, *112*(51), 15725–15730. https://doi.org/10.1073/pnas.1509557112

1127 Gibson, D. G., Young, L., Chuang, R.-Y., Venter, J. C., Hutchison, C. A., & Smith, H. O.

1128   (2009). Enzymatic assembly of DNA molecules up to several hundred kilobases.

1129   *Nature Methods*, *6*(5), 343–345. https://doi.org/10.1038/nmeth.1318

1130 Holm, L. (2020). DALI and the persistence of protein shape. *Protein Science: A Publication*

1131   *of the Protein Society*, *29*(1), 128–140. https://doi.org/10.1002/pro.3749

1132 Horsburgh, M. J., Aish, J. L., White, I. J., Shaw, L., Lithgow, J. K., & Foster, S. J. (2002). σB

1133   Modulates Virulence Determinant Expression and Stress Resistance: Characterization

1134   of a Functional rsbU Strain Derived from Staphylococcus aureus 8325-4. *Journal of*

1135   *Bacteriology*, *184*(19), 5457–5467. https://doi.org/10.1128/JB.184.19.5457-

1136   5467.2002

1137 Hudson, K. L., Bartlett, G. J., Diehl, R. C., Agirre, J., Gallagher, T., Kiessling, L. L., &

1138   Woolfson, D. N. (2015). Carbohydrate-Aromatic Interactions in Proteins. *Journal of*

1139   *the American Chemical Society*, *137*(48), 15152–15160.

1140   https://doi.org/10.1021/jacs.5b08424

1141 Hutter, J. L., & Bechhoefer, J. (1993). Calibration of atomic-force microscope tips. *Review of*

1142   *Scientific Instruments*, *64*(7), 1868–1873. https://doi.org/10.1063/1.1143970

1143   Kabsch, W. (2010). XDS. *Acta Crystallographica. Section D, Biological Crystallography*,

1144   *66*(Pt 2), 125–132. https://doi.org/10.1107/S0907444909047337

1145   Karimova, G., Ullmann, A., & Ladant, D. (2001). Protein-protein interaction between

1146   Bacillus stearothermophilus tyrosyl-tRNA synthetase subdomains revealed by a

1147   bacterial two-hybrid system. *Journal of Molecular Microbiology and Biotechnology*,

1148   *3*(1), 73–82.

1149   Kreiswirth, B. N., Löfdahl, S., Betley, M. J., O'Reilly, M., Schlievert, P. M., Bergdoll, M. S.,

1150   & Novick, R. P. (1983). The toxic shock syndrome exotoxin structural gene is not

1151   detectably transmitted by a prophage. *Nature*, *305*(5936), 709–712.

1152   https://doi.org/10.1038/305709a0

1153   Krissinel, E., & Henrick, K. (2007). Inference of macromolecular assemblies from crystalline

1154   state. *Journal of Molecular Biology*, *372*(3), 774–797.

1155   https://doi.org/10.1016/j.jmb.2007.05.022

1156   Kuru, E., Radkov, A., Meng, X., Egan, A., Alvarez, L., Dowson, A., Booher, G., Breukink,

1157   E., Roper, D. I., Cava, F., Vollmer, W., Brun, Y., & VanNieuwenhze, M. S. (2019).

1158   Mechanisms of Incorporation for D-Amino Acid Probes That Target Peptidoglycan

1159   Biosynthesis. *ACS Chemical Biology*, *14*(12), 2745–2756.

1160   https://doi.org/10.1021/acschembio.9b00664

1161   Lee, C. Y., Buranen, S. L., & Ye, Z. H. (1991). Construction of single-copy integration

1162   vectors for Staphylococcus aureus. *Gene*, *103*(1), 101–105.

1163   https://doi.org/10.1016/0378-1119(91)90399-v

1164   Liebschner, D., Afonine, P. V., Baker, M. L., Bunkóczi, G., Chen, V. B., Croll, T. I., Hintze,

1165   B., Hung, L. W., Jain, S., McCoy, A. J., Moriarty, N. W., Oeffner, R. D., Poon, B. K.,

1166   Prisant, M. G., Read, R. J., Richardson, J. S., Richardson, D. C., Sammito, M. D.,

1167   Sobolev, O. V., … Adams, P. D. (2019). Macromolecular structure determination

1168   using X-rays, neutrons and electrons: Recent developments in Phenix. *Acta*

1169   *Crystallographica. Section D, Structural Biology*, *75*(Pt 10), 861–877.

1170   https://doi.org/10.1107/S2059798319011471

1171 Loskill, P., Pereira, P. M., Jung, P., Bischoff, M., Herrmann, M., Pinho, M. G., & Jacobs, K.

1172   (2014). Reduction of the peptidoglycan crosslinking causes a decrease in stiffness of

1173   the Staphylococcus aureus cell envelope. *Biophysical Journal*, *107*(5), 1082–1089.

1174   https://doi.org/10.1016/j.bpj.2014.07.029

1175 Lund, V. A., Wacnik, K., Turner, R. D., Cotterell, B. E., Walther, C. G., Fenn, S. J., Grein,

1176   F., Wollman, A. J., Leake, M. C., Olivier, N., Cadby, A., Mesnage, S., Jones, S., &

1177   Foster, S. J. (2018). Molecular coordination of Staphylococcus aureus cell division.

1178   *ELife*, *7*, e32057. https://doi.org/10.7554/eLife.32057

1179 Maurer, P., Todorova, K., Sauerbier, J., & Hakenbeck, R. (2012). Mutations in Streptococcus

1180   pneumoniae penicillin-binding protein 2x: Importance of the C-terminal penicillin-

1181   binding protein and serine/threonine kinase-associated domains for beta-lactam

1182   binding. *Microbial Drug Resistance (Larchmont, N.Y.)*, *18*(3), 314–321.

1183   https://doi.org/10.1089/mdr.2012.0022

1184 McCoy, A. J., Grosse-Kunstleve, R. W., Adams, P. D., Winn, M. D., Storoni, L. C., & Read,

1185   R. J. (2007). Phaser crystallographic software. *Journal of Applied Crystallography*,

1186   *40*(Pt 4), 658–674. https://doi.org/10.1107/S0021889807021206

1187 Meeske, A. J., Riley, E. P., Robins, W. P., Uehara, T., Mekalanos, J. J., Kahne, D., Walker,

1188   S., Kruse, A. C., Bernhardt, T. G., & Rudner, D. Z. (2016). SEDS proteins are a

1189   widespread family of bacterial cell wall polymerases. *Nature*, *537*(7622), 634–638.

1190   https://doi.org/10.1038/nature19331

1191 Mir, M., Asong, J., Li, X., Cardot, J., Boons, G.-J., & Husson, R. N. (2011). The

1192   Extracytoplasmic Domain of the Mycobacterium tuberculosis Ser/Thr Kinase PknB

1193   Binds Specific Muropeptides and Is Required for PknB Localization. *PLOS*

1194   *Pathogens*, *7*(7), e1002182. https://doi.org/10.1371/journal.ppat.1002182

1195   Morales Angeles, D., Macia-Valero, A., Bohorquez, L. C., & Scheffers, D.-J. (2020). The

1196   PASTA domains of Bacillus subtilis PBP2B strengthen the interaction of PBP2B with

1197   DivIB. *Microbiology (Reading, England)*, *166*(9), 826–836.

1198   https://doi.org/10.1099/mic.0.000957

1199   Neuhaus, F. C., & Baddiley, J. (2003). A continuum of anionic charge: Structures and

1200   functions of D-alanyl-teichoic acids in gram-positive bacteria. *Microbiology and*

1201   *Molecular Biology Reviews: MMBR*, *67*(4), 686–723.

1202   https://doi.org/10.1128/mmbr.67.4.686-723.2003

1203   Novick, R. P., & Morse, S. I. (1967). In vivo transmission of drug resistance factors between

1204   strains of Staphylococcus aureus. *The Journal of Experimental Medicine*, *125*(1), 45–

1205   59. https://doi.org/10.1084/jem.125.1.45

1206   Panchal, V. V., Griffiths, C., Mosaei, H., Bilyk, B., Sutton, J. A. F., Carnell, O. T., Hornby,

1207   D. P., Green, J., Hobbs, J. K., Kelley, W. L., Zenkin, N., & Foster, S. J. (2020).

1208   Evolving MRSA: High-level β-lactam resistance in Staphylococcus aureus is

1209   associated with RNA Polymerase alterations and fine tuning of gene expression. *PLoS*

1210   *Pathogens*, *16*(7), e1008672. https://doi.org/10.1371/journal.ppat.1008672

1211   Pasquina-Lemonche, L., Burns, J., Turner, R. D., Kumar, S., Tank, R., Mullin, N., Wilson, J.

1212   S., Chakrabarti, B., Bullough, P. A., Foster, S. J., & Hobbs, J. K. (2020). The

1213   architecture of the Gram-positive bacterial cell wall. *Nature*, *582*(7811), 294–297.

1214   https://doi.org/10.1038/s41586-020-2236-6

1215   Pereira, S. F. F., Henriques, A. O., Pinho, M. G., de Lencastre, H., & Tomasz, A. (2007).

1216   Role of PBP1 in cell division of Staphylococcus aureus. *Journal of Bacteriology*,

1217   *189*(9), 3525–3531. https://doi.org/10.1128/JB.00044-07

1218   Pereira, S. F. F., Henriques, A. O., Pinho, M. G., de Lencastre, H., & Tomasz, A. (2009).

1219   Evidence for a dual role of PBP1 in the cell division and cell separation of

1220   Staphylococcus aureus. *Molecular Microbiology*, *72*(4), 895–904.

1221   https://doi.org/10.1111/j.1365-2958.2009.06687.x

1222   Pinho, M. G., de Lencastre, H., & Tomasz, A. (2001). An acquired and a native penicillin-

1223   binding protein cooperate in building the cell wall of drug-resistant staphylococci.

1224   *Proceedings of the National Academy of Sciences of the United States of America*,

1225   *98*(19), 10886–10891. https://doi.org/10.1073/pnas.191260798

1226   Pinho, M. G., & Errington, J. (2005). Recruitment of penicillin-binding protein PBP2 to the

1227   division site of Staphylococcus aureus is dependent on its transpeptidation substrates.

1228   *Molecular Microbiology*, *55*(3), 799–807. https://doi.org/10.1111/j.1365-

1229   2958.2004.04420.x

1230   Pinho, M. G., Filipe, S. R., de Lencastre, H., & Tomasz, A. (2001). Complementation of the

1231   essential peptidoglycan transpeptidase function of penicillin-binding protein 2 (PBP2)

1232   by the drug resistance protein PBP2A in Staphylococcus aureus. *Journal of*

1233   *Bacteriology*, *183*(22), 6525–6531. https://doi.org/10.1128/JB.183.22.6525-

1234   6531.2001

1235   Pinho, M. G., Kjos, M., & Veening, J.-W. (2013). How to get (a)round: Mechanisms

1236   controlling growth and division of coccoid bacteria. *Nature Reviews. Microbiology*,

1237   *11*(9), 601–614. https://doi.org/10.1038/nrmicro3088

1238   Reed, P., Atilano, M. L., Alves, R., Hoiczyk, E., Sher, X., Reichmann, N. T., Pereira, P. M.,

1239   Roemer, T., Filipe, S. R., Pereira-Leal, J. B., Ligoxygakis, P., & Pinho, M. G. (2015).

1240   Staphylococcus aureus Survives with a Minimal Peptidoglycan Synthesis Machine

1241   but Sacrifices Virulence and Antibiotic Resistance. *PLoS Pathogens*, *11*(5),

1242   e1004891. https://doi.org/10.1371/journal.ppat.1004891

1243   Reichmann, N. T., Tavares, A. C., Saraiva, B. M., Jousselin, A., Reed, P., Pereira, A. R.,

1244   Monteiro, J. M., Sobral, R. G., VanNieuwenhze, M. S., Fernandes, F., & Pinho, M. G.

1245   (2019). SEDS-bPBP pairs direct lateral and septal peptidoglycan synthesis in

1246   Staphylococcus aureus. *Nature Microbiology*, *4*(8), 1368–1377.

1247   https://doi.org/10.1038/s41564-019-0437-2

1248   Ruggiero, A., Squeglia, F., Marasco, D., Marchetti, R., Molinaro, A., & Berisio, R. (2011).

1249   X-ray structural studies of the entire extracellular region of the serine/threonine kinase

1250   PrkC from Staphylococcus aureus. *The Biochemical Journal*, *435*(1), 33–41.

1251   https://doi.org/10.1042/BJ20101643

1252   Sader, J. E., Borgani, R., Gibson, C. T., Haviland, D. B., Higgins, M. J., Kilpatrick, J. I., Lu,

1253   J., Mulvaney, P., Shearer, C. J., Slattery, A. D., Thorén, P.-A., Tran, J., Zhang, H.,

1254   Zhang, H., & Zheng, T. (2016). A virtual instrument to standardise the calibration of

1255   atomic force microscope cantilevers. *Review of Scientific Instruments*, *87*(9), 093711.

1256   https://doi.org/10.1063/1.4962866

1257   Sambrook, J., Fritsch, E. F., & Maniatis, T. (1989). Molecular cloning: A laboratory manual.

1258   *Molecular Cloning: A Laboratory Manual.*, *Ed. 2*.

1259   https://www.cabdirect.org/cabdirect/abstract/19901616061

1260   Saraiva, B. M., Sorg, M., Pereira, A. R., Ferreira, M. J., Caulat, L. C., Reichmann, N. T., &

1261   Pinho, M. G. (2020). Reassessment of the distinctive geometry of Staphylococcus

1262   aureus cell division. *Nature Communications*, *11*(1), 4097.

1263   https://doi.org/10.1038/s41467-020-17940-9

1264   Schenk, S., & Laddaga, R. A. (1992). Improved method for electroporation of

1265   Staphylococcus aureus. *FEMS Microbiology Letters*, *73*(1–2), 133–138.

1266   https://doi.org/10.1016/0378-1097(92)90596-g

1267   Schneider, T., & Sahl, H.-G. (2010). An oldie but a goodie—Cell wall biosynthesis as

1268   antibiotic target pathway. *International Journal of Medical Microbiology: IJMM*,

1269   *300*(2–3), 161–169. https://doi.org/10.1016/j.ijmm.2009.10.005

1270   Shah, I. M., Laaberki, M.-H., Popham, D. L., & Dworkin, J. (2008). A Eukaryotic-like

1271   Ser/Thr Kinase Signals Bacteria to Exit Dormancy in Response to Peptidoglycan

1272   Fragments. *Cell*, *135*(3), 486–496. https://doi.org/10.1016/j.cell.2008.08.039

1273   Silhavy, T. J., Kahne, D., & Walker, S. (2010). The bacterial cell envelope. *Cold Spring*

1274   *Harbor Perspectives in Biology*, *2*(5), a000414.

1275   https://doi.org/10.1101/cshperspect.a000414

1276   Squeglia, F., Marchetti, R., Ruggiero, A., Lanzetta, R., Marasco, D., Dworkin, J., Petoukhov,

1277   M., Molinaro, A., Berisio, R., & Silipo, A. (2011). Chemical Basis of Peptidoglycan

1278   Discrimination by PrkC, a Key Kinase Involved in Bacterial Resuscitation from

1279   Dormancy. *Journal of the American Chemical Society*, *133*(51), 20676–20679.

1280   https://doi.org/10.1021/ja208080r

1281   Srisuknimit, V., Qiao, Y., Schaefer, K., Kahne, D., & Walker, S. (2017). Peptidoglycan

1282   Cross-Linking Preferences of Staphylococcus aureus Penicillin-Binding Proteins

1283   Have Implications for Treating MRSA Infections. *Journal of the American Chemical*

1284   *Society*, *139*(29), 9791–9794. https://doi.org/10.1021/jacs.7b04881

1285   Steele, V. R., Bottomley, A. L., Garcia-Lara, J., Kasturiarachchi, J., & Foster, S. J. (2011).

1286   Multiple essential roles for EzrA in cell division of Staphylococcus aureus. *Molecular*

1287   *Microbiology*, *80*(2), 542–555. https://doi.org/10.1111/j.1365-2958.2011.07591.x

1288   Straume, D., Piechowiak, K. W., Olsen, S., Stamsås, G. A., Berg, K. H., Kjos, M.,

1289   Heggenhougen, M. V., Alcorlo, M., Hermoso, J. A., & Håvarstein, L. S. (2020). Class

1290   A PBPs have a distinct and unique role in the construction of the pneumococcal cell

1291   wall. *Proceedings of the National Academy of Sciences of the United States of*

1292   *America*, *117*(11), 6129–6138. https://doi.org/10.1073/pnas.1917820117

1293 Studier, F. W., & Moffatt, B. A. (1986). Use of bacteriophage T7 RNA polymerase to direct

1294   selective high-level expression of cloned genes. *Journal of Molecular Biology*,

1295   *189*(1), 113–130. https://doi.org/10.1016/0022-2836(86)90385-2

1296 Su, H.-N., Li, K., Zhao, L.-S., Yuan, X.-X., Zhang, M.-Y., Liu, S.-M., Chen, X.-L., Liu, L.-

1297   N., & Zhang, Y.-Z. (2020). Structural Visualization of Septum Formation in

1298   Staphylococcus warneri Using Atomic Force Microscopy. *Journal of Bacteriology*,

1299   *202*(19). https://doi.org/10.1128/JB.00294-20

1300 Sutton, J. A. F., Carnell, O. T., Lafage, L., Gray, J., Biboy, J., Gibson, J. F., Pollitt, E. J. G.,

1301   Tazoll, S. C., Turnbull, W., Hajdamowicz, N. H., Salamaga, B., Pidwill, G. R.,

1302   Condliffe, A. M., Renshaw, S. A., Vollmer, W., & Foster, S. J. (2021).

1303   Staphylococcus aureus cell wall structure and dynamics during host-pathogen

1304   interaction. *PLoS Pathogens*, *17*(3), e1009468.

1305   https://doi.org/10.1371/journal.ppat.1009468

1306 Swoboda, J. G., Campbell, J., Meredith, T. C., & Walker, S. (2010). Wall teichoic acid

1307   function, biosynthesis, and inhibition. *Chembiochem: A European Journal of*

1308   *Chemical Biology*, *11*(1), 35–45. https://doi.org/10.1002/cbic.200900557

1309 Taguchi, A., Welsh, M. A., Marmont, L. S., Lee, W., Sjodt, M., Kruse, A. C., Kahne, D.,

1310   Bernhardt, T. G., & Walker, S. (2019). FtsW is a peptidoglycan polymerase that is

1311   functional only in complex with its cognate penicillin-binding protein. *Nature*

1312   *Microbiology*, *4*(4), 587–594. https://doi.org/10.1038/s41564-018-0345-x

1313 Turner, R. D., Ratcliffe, E. C., Wheeler, R., Golestanian, R., Hobbs, J. K., & Foster, S. J.

1314   (2010). Peptidoglycan architecture can specify division planes in Staphylococcus

1315   aureus. *Nature Communications*, *1*, 26. https://doi.org/10.1038/ncomms1025

1316 Turner, R. D., Vollmer, W., & Foster, S. J. (2014). Different walls for rods and balls: The

1317   diversity of peptidoglycan. *Molecular Microbiology*, *91*(5), 862–874.

1318   https://doi.org/10.1111/mmi.12513

1319 Typas, A., Banzhaf, M., Gross, C. A., & Vollmer, W. (2011). From the regulation of

1320   peptidoglycan synthesis to bacterial growth and morphology. *Nature Reviews.*

1321   *Microbiology*, *10*(2), 123–136. https://doi.org/10.1038/nrmicro2677

1322 Vollmer, W., Blanot, D., & de Pedro, M. A. (2008). Peptidoglycan structure and architecture.

1323   *FEMS Microbiology Reviews*, *32*(2), 149–167. https://doi.org/10.1111/j.1574-

1324   6976.2007.00094.x

1325 Weidenmaier, C., Peschel, A., Xiong, Y.-Q., Kristian, S. A., Dietz, K., Yeaman, M. R., &

1326   Bayer, A. S. (2005). Lack of wall teichoic acids in Staphylococcus aureus leads to

1327   reduced interactions with endothelial cells and to attenuated virulence in a rabbit

1328   model of endocarditis. *The Journal of Infectious Diseases*, *191*(10), 1771–1777.

1329   https://doi.org/10.1086/429692

1330 Winn, M. D., Ballard, C. C., Cowtan, K. D., Dodson, E. J., Emsley, P., Evans, P. R., Keegan,

1331   R. M., Krissinel, E. B., Leslie, A. G. W., McCoy, A., McNicholas, S. J., Murshudov,

1332   G. N., Pannu, N. S., Potterton, E. A., Powell, H. R., Read, R. J., Vagin, A., & Wilson,

1333   K. S. (2011). Overview of the CCP4 suite and current developments. *Acta*

1334   *Crystallographica. Section D, Biological Crystallography*, *67*(Pt 4), 235–242.

1335   https://doi.org/10.1107/S0907444910045749

1336 Yang, Y., Bhachech, N., & Bush, K. (1995). Biochemical comparison of imipenem,

1337   meropenem and biapenem: Permeability, binding to penicillin-binding proteins, and

1338   stability to hydrolysis by beta-lactamases. *The Journal of Antimicrobial*

1339   *Chemotherapy*, *35*(1), 75–84. https://doi.org/10.1093/jac/35.1.75

1340   Yeats, C., Finn, R. D., & Bateman, A. (2002). The PASTA domain: A beta-lactam-binding

1341   domain. *Trends in Biochemical Sciences*, *27*(9), 438. https://doi.org/10.1016/s0968-

1342   0004(02)02164-3

1343   Zapun, A., Contreras-Martel, C., & Vernet, T. (2008). Penicillin-binding proteins and beta-

1344   lactam resistance. *FEMS Microbiology Reviews*, *32*(2), 361–385.

1345   https://doi.org/10.1111/j.1574-6976.2007.00095.x

1346   Zhao, G., Meier, T. I., Kahl, S. D., Gee, K. R., & Blaszczak, L. C. (1999). BOCILLIN FL, a

1347   Sensitive and Commercially Available Reagent for Detection of Penicillin-Binding

1348   Proteins. *Antimicrobial Agents and Chemotherapy*, *43*(5), 1124–1128.

1349   Zhou, X., Halladin, D. K., Rojas, E. R., Koslover, E. F., Lee, T. K., Huang, K. C., & Theriot,

1350   J. A. (2015). Bacterial division. Mechanical crack propagation drives millisecond

1351   daughter cell separation in Staphylococcus aureus. *Science (New York, N.Y.)*,

1352   *348*(6234), 574–578. https://doi.org/10.1126/science.aaa1511

1353

1354 **Appendix Tables**

1355 **Appendix Table 1. Strains used in this study**

Name	Relevant genotype/Markers	Source
Staphylococcus aureus		
SH1000	Functional *rsbU*$^+$ derivative of *S. aureus* 8325-4	(Horsburgh et al., 2002)
VF17	SH1000 pGL485 (*lacI*); Cm^R	(Steele et al., 2011)
RN4220	Restriction deficient transformation recipient	(Kreiswirth et al., 1983)
CYL316	RN4220 pCL112Δ19	(Lee et al., 1991)
SJF4588	SH1000 *geh::Pspac-pbp1*; Tet^R	This study
SJF5116	SH1000 *geh::Pspac -pbp1 Δpbp1*; Tet^R	This study
SJF5275	SH1000 *geh::Pspac -pbp1 pbp1*$_{\Delta PASTA}$; Tet^R	This study
SJF4590	SH1000 *geh::Pspac -pbp1 pbp1** Tet^R, Cm^R	This study
Δpbp1	SH1000 *geh::Pspac -pbp1 Δpbp1 lacI*; Tet^R	This study
pbp1$_{\Delta PASTA}$	SH1000 *geh::Pspac -pbp1 pbp1*$_{\Delta PASTA}$ *lacI*; Tet^R, Cm^R	This study
*pbp1**	SH1000 *geh::Pspac -pbp1 pbp1* lacI*; Tet^R, Cm^R	This study
SJF5046	SH1000 *lysA::pmecA rpoB*^{H929Q}; Ery^R, Kan^R	(Panchal et al., 2020)
Δpbp1 p*mecA*	SH1000 *geh::Pspac-pbp1 Δpbp1 lacI lysA::pmecA*; Tet^R, Cm^R, Ery^R	This study
*pbp1** p*mecA*	SH1000 *geh::Pspac-pbp1 pbp1* lacI lysA::pmecA*; Tet^R, Cm^R, Ery^R	This study
MRSA *Δpbp1*	SH1000 *geh::Pspac-pbp1 Δpbp1 lacI lysA::pmecA rpoB*^{H929Q}; Tet^R, Cm^R, Ery^R, Kan^R	This study
MRSA *pbp1**	SH1000 *geh::Pspac-pbp1 pbp1* lacI lysA::pmecA rpoB*^{H929Q}; Tet^R, Cm^R, Ery^R, Kan^R	This study
JGL227	SH1000 *ezrA-gfp+*; Ery^R	(Steele et al., 2011)
Δpbp1 ezrA-gfp	SH1000 *geh::Pspac-pbp1 Δpbp1 lacI ezrA-gfp*; Tet^R, Cm^R, Ery^R	This study
pbp1$_{\Delta PASTA}$ *ezrA-gfp*	SH1000 *geh::Pspac-pbp1 pbp1*$_{\Delta PASTA}$ *lacI ezrA-gfp*; Tet^R, Cm^R, Ery^R	This study

pbp1* ezrA-gfp	SH1000 *geh::Pspac-pbp1 pbp1* lacI ezrA-gfp*; Tet^R, Cm^R, Ery^R	This study
NE420	JE2 *pbp3::Tn*; Ery^R	(Fey et al., 2013)
SH4421	SH1000 *pbp3::Tn*; Ery^R	This study
NE3004	RN4220 pKAN; Cm^R, Ery^R	(Fey et al., 2013)
SH4425	*pbp4::Tn*; Ery^R	(Lund et al., 2018)
SH5115	SH1000 *pbp4::kan*; Kan^R	This study
pbp3 pbp4 (SH5483)	*pbp3::Tn pbp4::kan*; Ery^R ,Kan^R,	This study
Δ*pbp1 pbp4*	SH1000 *geh::Pspac-pbp1* Δ*pbp1 lacI pbp4::Tn*; Tet^R, Cm^R, Kan^R	This study
pbp1$_{ΔPASTA}$ *pbp4*	SH1000 *geh::Pspac-pbp1 pbp1*$_{ΔPASTA}$ *lacI pbp4::Tn*; Tet^R, Cm^R, Kan^R	This study
pbp1* pbp4	SH1000 *geh::Pspac-pbp1 pbp1* lacI pbp4::Tn*; Tet^R, Cm^R, Kan^R	This study
tarO	SH1000 Δ*tarO::ery*; Ery^R	Constructed by Dr B. Salamaga (University of Sheffield)
tarO tarO+	SA113 Δ*tarO::ery* pUC1-*tarO* ; Ery^R, Cm^R	Constructed by Dr B. Salamaga (University of Sheffield)
Δ*pbp1 tarO*	SH1000 *geh::Pspac-pbp1* Δ*pbp1 lacI* Δ*tarO::ery*; Tet^R, Cm^R, Ery^R	This study
pbp1$_{ΔPASTA}$ *tarO*	SH1000 *geh::Pspac-pbp1 pbp1*$_{ΔPASTA}$ *lacI* Δ*tarO::ery*; Tet^R, Cm^R, Ery^R	This study
pbp1* tarO	SH1000 *geh::Pspac-pbp1 pbp1* lacI* Δ*tarO::ery*; Tet^R, Cm^R, Ery^R	This study
Escherichia coli		
NEB5α	*fhuA2 (argF-lacZ)U169 phoA glnV44 80 (lacZ)M15 gyrA96 recA1 relA1 endA1 thi-1 hsdR17*	New England Biolabs
BTH101	*F⁻, cya-99, araD139, galE15, galK16, rpsL1, hsdR2, mcrA1, mcrB1*	(Karimova et al., 2001)
Rosetta (DE3)	*F⁻ ompT hsdS*$_B$(r$_B$⁻ m$_B$⁻) *gal dcm* (DE3) pRARE (Cm^R)	Novagen
BL21(DE3)	F⁻ *ompT hsd*S$_B$ (r$_B$⁻, m$_B$⁻) *gal dcm* (DE3)	(Studier & Moffatt, 1986)

1356

73

1357 **Appendix Table 2. Plasmids used in this study**

Name	Characteristics	Source
pCQ11-FtsZ-SNAP	pCQ11 derivative containing *ftsZ-snap* under P*spac*; Amp^R, Ery^R	(Lund et al., 2018)
pKASBAR	pUC18 containing *attP* and tetracycline cassette; Amp^R, Tet^R	(Bottomley et al., 2014)
pKB-P*spac-pbp1*	pKASBAR containing *S. aureus pbp1* under P*spac*; Amp^R, Tet^R	This study
pMAD	*E. coli-S. aureus* shuttle vector with temperature-sensitive origin of replication in *S. aureus* and constitutively produced thermostable β-galactosidase encoded by *bgaB*; Amp^R, Ery^R	(Arnaud et al., 2004)
pMAD-Δ*pbp1*	pMAD containing a deletion cassette for *S. aureus pbp1*; Amp^R, Ery^R	This study
pMAD-*pbp1*$_{ΔPASTA}$	pMAD containing a deletion cassette for *S. aureus pbp1* PASTA domains; Amp^R, Ery^R	This study
pMAD-*pbp1**	pMAD containing a cassette for introduction of a point mutation (S314A) in the active site *S. aureus pbp1*; Amp^R, Ery^R	This study
pGL485	*E. coli-S. aureus* shuttle vector carrying *E. coli lacI* gene under the control of a constitutive promoter; Spec^R, Cam^R	(Cooper et al., 2009)
T18 (pUT18C)	Derivative of high copy-number pUC19, carrying gene encoding amino acids 225 to 399 of CyaA (T18 fragment); Amp^R	(Karimova et al., 2001)
T18-zip (pUT18C-zip)	pUT18C coding for the leucine zipper region of the GCN4 yeast protein. Positive control; Amp^R	(Karimova et al., 2001)
EzrA-T18 (pVF32)	pUT18(Karimova et al., 2001) containing T18 fused in frame to the 3′ end of *S. aureus ezrA*; Amp^R	(Steele et al., 2011)
T18-PBP2 (pGL547)	pUT18C containing T18 fused in frame to the 5′ end of *S. aureus pbp2*; Amp^R	(Steele et al., 2011)
T18-DivIC (pGL564)	pUT18C containing T18 fused in frame to the 5′ end of *S. aureus divIC*; Amp^R	(Steele et al., 2011)
T18-DivIB (pGL544)	pUT18C containing T18 fused in frame to the 5′ end of *S. aureus divIB*; Amp^R	(Steele et al., 2011)
T18-FtsW (pALB6)	pUT18C containing T18 fused in frame to the 5′ end of *S. aureus ftsW*; Amp^R	(Steele et al., 2011)
T25 (pKT25)	Derivative of low copy-number pSU40, carrying the first 224 amino acids of *B. subtilis* CyaA (T25 fragment); Kan^R	(Karimova et al., 2001)

T25-zip (pKT25-zip)	pKT25 coding for the leucine zipper region of the GCN4 yeast protein. Positive control; Kan[R]	(Karimova et al., 2001)
T25-PBP1 (pGL550)	pKT25 containing T25 fused in frame to the 5′ end of *S. aureus pbp1*; Kan[R]	(Steele et al., 2011)
T25-PBP1$_{\Delta PASTA}$	pKT25 containing T25 fused in frame to the 5′ end of *S. aureus pbp1*$_{\Delta PASTA}$ (M1-S595); Kan[R]	This study
pOPINRSF	*kan* P$_{T7}$ *lacI*; Kan[R]	(Berrow et al., 2009)
pVR01	*kan* P$_{T7}$ *pbp1 lacI*; pOPINRSF derivative for overexpression of full length *S. aureus* PBP1 (1-744); Kan[R]	This study
pVR02	*kan* P$_{T7}$ *pbp1(37-744) lacI*; pOPINRSF derivative for overexpression of *Sa*PBP1 (37-744); Kan[R]	This study.
pVR03	*kan* P$_{T7}$ *pbp1*(37-744*: S314A) lacI*; pOPINRSF derivative for overexpression of *Sa*PBP1* (37-744); Kan[R]	This study
pVR04	*kan* P$_{T7}$ *pbp1(37-595) lacI*; pOPINRSF derivative for overexpression of *Sa*PBP1$_{\Delta PASTA}$(37-595); Kan[R]	This study
pVR06	*kan* P$_{T7}$ *pbp1(595-744) lacI*; pOPINRSF derivative for overexpression of *Sa*PASTA$_{PBP1}$ (595-744); Kan[R]	This study
pOPINJB	*bla* P$_{T7}$ *lacI*; Amp[R]	(Berrow et al., 2009)
pSA50	pOPINJB derivative for overexpression of sPBP1A-BAP; Amp[R]	This study

1358

75

1359 **Appendix Table 3. Oligonucleotides used in this study**

Name	5′-3′ oligonucleotide sequence
pCQ-pbp1-F	AGAAGGAGATATACATATGGCTTGAGAACGATAATGTAAAG
pCQ-pbp1-F	TATTATGCATTTAGAATAGGTTAGTCCGACTTATCCTTG
pKB-Pspac-pbp1-F	CCTTTTTTTGCCCCGGGATCCGCAAAAAGTTGTTGACTTTATC
pKB-Pspac-pbp1-R	CTATGACCATGATTACGAATTCTTAGTCCGACTTATCCTTG
pbp1-A	CCATGGTACCCGGGAGCTCGCACCATGACGCAACATTAG
pbp1-B	ATCCTTGTCATTAATTTTTTGCTTCGCC
pbp1-C	CAAAAAATTAATGACAAGGATAAGTCGGAC
pbp1-D	CCTCGCGTCGGGCGATATCGATCTCCCATAAACACTTTAGC
pbp1-E	CCATGGTACCCGGGAGCTCGAATTCTAAAAAACCTAGGCATG
pbp1-F	TATCCTTGTCAGATGTGTCATCTTTTGATTTAC
pbp1-G	TGACACATCTGACAAGGATAAGTCGGACTAAC
pbp1-H	GCGTCTGCAGAAGCTTCTAGTTAATGCACTCCAATCCATAAAC
pbp1*5′-F	CCATGGTACCCGGGAGCTCGAATTCAGTATACCGAAGCAACAACCAC
pbp1*5′-R	TTAAATGTTGCTCCAGGCTCGTATGTGTTTTG
pbp1*3′-F	GAGCCTGGAGCAACATTTAAATCAT ATGGGTTA
pbp1*3′-R	CCTCGCGTCGGGCGATATCGGATCCTTAGTCCGACTTATCCTTGTC
T25-pbp1-F	CTGCAGGGTCGACTCTAGAGATGGCGAAGCAAAAAATTAAAATTAAAAAAAATAAAATAG
T25-pbp1pasta-R	ACGTTGTAAAACGACGGCCGTTAAGATGTGTCATCTTTTGATTTACCTACATTTAAATATTTC
VR47F	AAGTTCTGTTTCAGGGCCCGGCGAAGCAGAAGATCAAGATTAAGAAAAAC
VR47R	ATGGTCTAGAAAGCTTTAATCGCTTTTATCCTTGTCGGTTTTGC
VR49F	ATGATTACCGGCCACAGCAAC
VR49R	CGGGCCCTGAAACAGAACTTCCAG
VR51	AACACCTATGAGCCGGGCGCCACCTTCAAAAGCTATGGTC
VR53	GAGCAAAGACGATACCAGCTAAGCGGAGTACAGCAAGG
VR57F	AGCAACGCGGAGTACAGCAAGGTGCCGGACGTTG

76

OPPF20018F	AAGTTCTGTTTCAGGGCCCGGCGAACGAGAAATACCTGGTTAAGAACGCGC
OPPF20018R	AGATGTCGTTCAGGCCATCGCTTTTATCCTTGTCGGTTTTGCTGTCGC

1360

1361 **Appendix Table 4. Crystallographic data**

	*Sa*PASTA$_{PBP1}$
Data	
Resolution (Å)	1.78
Space group	$P2_12_12_1$
a, b, c (Å)	39.8, 81.4, 89.6
α, β, γ (°)	90, 90, 90
$<I/\sigma I>$[a]	14.2 (2.0)
Completeness (%)[a]	99.9 (99.8)
Redundancy[a]	7.7 (6.7)
$R_{p.i.m}$ (%)[a]	3.0 (39.1)
R_{merge} (%)[a]	6.0 (66.0)
CC$_{1/2}$[a]	99.8 (92.3)
Refinement	
R_{work} (%)	18.7 %
R_{free} (%)[b]	21.0 %
No. of residues	Chain A: 116, Chain B: 117
No. of waters	123
Average B-factor (Å^2)	
Protein	Chain A: 45.1, Chain B: 48.0
Waters	47.6
R.m.s.d on ideal values	
Bond lengths (Å)	0.005
Bond angle (°)	0.755
Ramachandran	
Most favoured (%)	98.69
Additional allowed (%)	1.31
Outliers (%)	0.0
PDB ID	7O61

1362 [a]Values in parentheses are for the highest resolution shell.

1363 [b]For determination of R_{free}, 5 % of reflections were randomly selected before refinement.